Global seasonal precipitation anomalies robustly associated with El Niño and La Niña events – an OLR perspective.

Andrew M. Chiodi[1]

Joint Institute for the Study of the Ocean and Atmosphere, University of Washington, Seattle, WA

D. E. Harrison

NOAA Pacific Marine Environmental Laboratory, Seattle, WA

and

JISAO, Univ. of WA, Seattle, WA

[1]*Corresponding author address:* Andrew Chiodi, JISAO University of Washington, 7600 Sand Point Way NE, Seattle, WA, 98115, U.S.A.
E-mail: andy.chiodi@noaa.gov

Abstract

El Niño-Southern Oscillation (ENSO) events are associated with particular seasonal weather anomalies in many regions around the planet. When the statistical links are sufficiently strong, ENSO state information can provide useful seasonal forecasts with varying lead times. However, using conventional Sea Surface Temperature or Sea Level Pressure indices to characterize ENSO state leads to many instances of limited forecast skill (e.g. years identified as 'El Niño' or 'La Niña' with weather anomalies unlike the average) even in regions where there is considerable ENSO-associated anomaly, on average. We show here that using outgoing longwave radiation (OLR) conditions to characterize ENSO state identifies a subset of the conventional ENSO years, which we call OLR-El Niño and OLR-La Niña years. Treating the OLR-identified subset of years differently can usefully strengthen both the level of statistical significance in the average (composite) and also greatly reduce the year-to-year deviations from the composite for precipitation anomalies. The OLR-El Niño index has been introduced previously, but the OLR-La Niña index introduced here is novel. Each index is motivated by our phenomenological understanding of El Niño and La Niña conditions. We also demonstrate that on average over most of the planet (particularly away from the western tropical Pacific), the non-OLR El Niño and non-OLR La Niña years have much more limited statistical utility for precipitation. Understanding better how large scale environmental conditions during ENSO events determine OLR (and deep-atmospheric convection) conditions will lead to improved seasonal precipitation forecasts for many areas.

1. Introduction

Definitions for the warm (El Niño) and cold (La Niña) phases of the El Niño-Southern Oscillation (ENSO) based on tropical Pacific surface marine conditions have been used previously to reveal the now well-known statistical links between ENSO and seasonal weather anomalies around the globe (see, for example, the seminal seasonal precipitation and temperature composites described by Ropelewski and Halpert, 1986, 1987, 1989; and Halpert and Ropelewski, 1992). These links provide an important basis for skillful statistical seasonal weather prediction where they are strong enough (Kiladis and Diaz 1989, Wolter et al. 1999, Smith et al. 1999). It has become clear, however, that even in the most strongly affected regions, many years identified as "El Niño" or "La Niña" based on the now commonly used SSTA-based ENSO definitions do not have seasonal weather anomaly patterns that match those seen on average (e.g., Harrison and Larkin, 1998; Larkin and Harrison, 2005a, b). Seasonal weather anomalies may not in general be simply and strongly related to ENSO (Kumar et al., 2007) as it has been conventionally defined. We show here that a different perspective on ENSO conditions can improve the statistical weather associations on which much seasonal forecasting is based.

Outgoing longwave radiation (OLR), sea level pressure (SLP) and sea surface temperature (SST) all provide measures of the state of the coupled-ENSO system, but of these OLR has the closest connection to the atmospheric heating anomalies that drive atmospheric circulation anomalies elsewhere. OLR in the deep tropics is strongly influenced by the presence (or absence) of deep-atmospheric convection activity. It is a commonly held notion that tropical Pacific deep-atmospheric convection activity spreads eastward during the transition to El Niño state (as depicted in the familiar ENSO cartoons; see Fig. 1). Chiodi and Harrison (2010) looked

62 for this spread in convection using OLR and found that the strikingly low OLR anomalies that
63 are indicative of significant amounts of deep atmospheric convective activity in the tropics are
64 clearly observed in the eastern central Pacific during some, but not all, of the years that are
65 commonly considered to be El Niño years based on the commonly used SSTA-based ENSO
66 definitions. Whereas ENSO SSTA (e.g. the NIÑO 3.4 index) follows a continuous distribution,
67 the (anomalously low) OLR peaks seen in these years are well separated from the background
68 variability seen in this region at other times (see Chiodi and Harrison, 2008 and 2010; also Fig.
69 3a). Thus, the OLR El Niño index clearly picks out a subset of the years commonly identified
70 years.

71 With focus on the U.S., Chiodi and Harrison (2013) showed that the years identified by
72 the OLR-El Niño index yield composite seasonal weather anomalies with familiar patterns
73 (broadly resembling those described in previous period ENSO studies), high levels of statistical
74 significance (based on amplitude), and surprising year-to-year consistency. Composites based
75 on all of the years commonly identified as El Niño were also shown to have patterns shaped like
76 those seen in the OLR-El Niño composite, but at considerably weaker amplitude. The other
77 "non-OLR El Niño" years yielded composite seasonal weather anomalies with very little
78 statistically significant anomaly over the U.S. and a high degree of year-to-year deviation. Thus,
79 from a seasonal weather forecasting perspective, most of the useful impacts of El Niño on the
80 U.S. are due to the years identified by the Chiodi and Harrison (2013) OLR El Niño index.

81 Motivated by the success of the Chiodi and Harrison (2013) results, we herein identify a
82 novel OLR index for La Niña. Our approach to using OLR information in this case (as described
83 in more detail in the Data and Methods section, below) was motivated by our phenomenological
84 understanding of La Niña atmospheric convection conditions (e.g. Fig 1). Like its warm-ENSO

counterpart, the OLR La Niña index rather clearly identifies some but not all of the years with ENSO status based on the NOAA historical ENSO definition (which is based on five consecutive months of the 3-month running average Niño 3.4 SSTA amplitude exceeding 0.5°C). The relationship between the OLR La Niña index and global seasonal precipitation anomaly is examined here mainly using composite analysis. We also extend the Chiodi and Harrison (2013) composite analysis methodology, which was used to just look at relationships over the contiguous U.S., to global precipitation and atmospheric circulation anomalies over the period for which satellite-based OLR information is available (period 1974 to 2011).

We describe the seasonally averaged composite anomalies of tropical Pacific OLR and continental precipitation based on the identified OLR La Niña and OLR El Niño years, and examine these composites for their local statistical significance and robustness (event-to-event consistency in pattern). In the precipitation case, we also examine the global, or overall "field" significance (e.g. Livezey and Chen, 1983; Wilks, 2006) of the composites. We do this by answering the question of whether or not the composites contain (sufficiently) more locally statistically significant anomaly than should be expected based on chance (e.g. random selection of years) alone. We compare the OLR-event composites to others based just on the non-OLR El Niño and non-OLR La Niña years. The OLR perspective on ENSO is shown to strengthen (increase anomaly amplitude, decrease year-to-year deviation) the continental precipitation composites.

2. Data and Methods

We use daily ``Interpolated OLR" averages provided by NOAA/OAR/ESRL Physical Sciences Division, Boulder, Colorado, USA, from their Web site at http://www.cdc.noaa.gov/. This is a satellite-derived product available on a 2.5x2.5 degree grid. Details of the interpolation technique are described by Liebmann and Smith (1996). Daily OLR averages are available from July 1974 to the present with a gap in coverage from March to December of 1978. Because of this gap, the 1978-79 period is omitted from consideration here.

In the tropics, large shifts in the satellite-measured OLR are associated with transitions from relatively clear sky conditions, in which OLR is dominated by surface longwave radiation, to deep convective conditions, in which OLR is influenced mainly by radiation from the cooler deep-cloud tops (e.g., Trenberth et al. 1998). Absolute OLR measurements less than 230 W m^{-2} have previously been used as a proxy for deep tropical convection (Garreaud and Wallace 1997), with values substantially larger than that indicative of a lack of deep atmospheric convection activity (“clear sky”).

The Chiodi and Harrison (2013) OLR index for El Niño (as described in the introduction) is based on monthly OLR anomaly behavior averaged over the region bounded by 160°W-110°W and 5°S-5°N. To calculate the OLR El Niño index, the daily average OLR data is first filtered with a 30-day running mean filter and anomalies are determined by removing the linearly-interpolated climatological monthly average. A climatological base period of 1974-2011 (the study period) is used throughout this paper.

For La Niña, our initial approach to using OLR was also motivated by the notions illustrated in the familiar ENSO cartoons (Fig. 1), as well as a quick look at the corresponding long-time-average OLR observations (Fig. 2). The difference between OLR averaged over all

times falling into the La Niña state minus the average over all ENSO-neutral times (defined here in a preliminary manner using NIÑO3.4 SSTA) shows tropical Pacific extrema centered mainly over two regions, those being the Island Nations of the far western tropical Pacific (where OLR decreases – indicative of deep-convection activity increases – are seen) and a region west of the Date Line, in which OLR increases (from which we infer a reduction in deep-atmospheric convection activity) are seen.

We looked at monthly averaged OLR behavior spatially averaged over the Island Nations but found time series that exhibit troughs (negative peaks) of comparable amplitude over a variety of time scales (including in years not commonly considered El Niño or La Niña). Apparently, there are many sources of variability besides ENSO that control monthly averaged OLR behavior here. Monthly averaged OLR in the western tropical Pacific (we focus here on the region bounded by 150°E to 180° and 5°S to 5°N) does exhibit substantial interannual peaks, but they are seen not only in some of the years commonly considered to be La Niña years, but also in the mature stage of some of the stronger El Niño years (these type of peaks occur as the convection spreads eastward, rather than westward). Thus, looking at monthly averaged OLR behavior over this region leads us to an ambiguous indicator of ENSO-related activity.

We have found that looking instead at synoptic timescale behavior over the western Tropical Pacific provides an interesting perspective on the processes involved in the initiation and growth of the La Niña anomaly state. Particularly, we find that the occurrence of clear sky-type conditions in daily averaged OLR over this region are typically associated with synoptic time scale increases in the strength of the underlying near surface easterly winds. We find that these easterly wind increases that have strength within the oceanic waveguide (within a few degrees from the Equator) have the effect, on average, of driving cooling of the oceanic waveguide that

151 persists over the following couple months. We also find that the chance of seeing another
152 easterly wind surge in the near future (e.g. following month) substantially increases as the
153 waveguide cools. This suggests that synoptic scale atmospheric processes involving reduced
154 convection in the western tropical Pacific and underlying increases in the predominantly easterly
155 near surface equatorial winds provide an important mechanism for La Niña initiation and growth
156 The observed changes in SSTA following these easterly wind surges, as well as their effects on
157 ocean models and their distribution with observed ENSO-SSTA is described in a paper
158 submitted recently by us to this journal.

159

160 Informed by these findings, the OLR-based index we have chosen to examine in this case
161 depends upon the occurrence (in a running-sum sense) of clear sky conditions in the central
162 tropical Pacific, with focus on the region from 150°E to 180°. More specifically, the OLR La
163 Niña index (OLNI) is defined based on daily average OLR conditions as,

$$OLNI(n) = \sum_{i=1}^{n} C(i)$$

164 with

165

$$C(i) = \begin{cases} 1 \; if \; OLR(i) > OLRc \\ 0 \; otherwise \end{cases}$$

166

167 where *n* and *i* are the number of days since 1 April of ENSO Year 0 (the index running-sum
168 begins then, in each year), *OLR(i)* is the daily average OLR value averaged over the region
169 bounded by 150°E, 180° and 5°S, 5°N, and *OLRc* is 265 W m^{-2}, which in this region is the 95th

percentile "clear sky" value. The OLR La Niña index with *n* corresponding to 31 December of Year 0 is shown in Figure 3b. For the compositing analysis described here, we define OLR La Niña years as the years in which the OLR La Niña index crosses the 30 day threshold. There is a discontinuity of about a half of a time series standard deviation that is seen around 30 days in the ranked-distribution of the yearly index values. The ranked-distribution is basically continuous until then (the largest prior jump between consecutively ranked values is less than 0.25 standard deviations). This value is crossed only in six years, even if the index is extended (*n* is increased) through May of ENSO Year 1. The dates in which this index first crosses the 30 day threshold in each of these six years are listed in Table 1. We find that small changes in the index averaging parameters, such as using meridional bounds of 4° rather than 5°, or going to 200°E rather than 180°, or using the 90th percentile daily OLR value (260 W m $^{-2}$) as threshold instead of the 95th can have the effects of changing the scale of the index somewhat, but the qualitative relationship between the years remains the same (for example, based on the 90th percentile threshold, the same 6 years are identified and there still is a ~½ sigma gap between the 7th and 6th highest-ranked year, but it occurs around 55 days, rather than 30 days).

Here, "ENSO Year" is taken as defined in previous compositing studies (Rasmussen and Carpenter 1983, Larkin and Harrison 2002), with Year 0 typically corresponding to the development and beginnings of the mature stage of ENSO (e.g. 1997 of the large 1997-98 El Niño event) and Year 1 the following. Peak tropical Pacific anomaly conditions typically occur around the end of Year 0 or beginning of Year 1.

Following Chiodi and Harrison (2013), we also define "non-OLR La Niña" years as the other years that are identified as La Niña years based on the current NOAA definition, but are

not identified by the OLR La Niña index. There are also six such non-OLR La Niña years in the period considered (marked by unfilled blue arrows in Fig. 3c).

Monthly mean Global Precipitation Climatology Center (GPCC) Precipitation data (v4) were obtained from the NOAA/OAR/ESRL PSD, Boulder, Colorado, USA, from their Web site at http://www.esrl.noaa.gov/psd/. More information about this gauge-based gridded precipitation data set is available from the GPCC homepage http://gpcc.dwd.de and Rudolf and Schneider (2005; 2010).

The SSTA data used herein (including to calculate the Niño3.4 index) was provided by the U.K. Met Office's Hadley Centre (see Rayner et al. 2003 for discussion of the Hadley Centre "HadISST" data set), from their website at http://www.metoffice.gov.uk/hadobs/hadisst/.

3. OLR Indices

OLR behavior in the OLR EL Niño index region is characterized by its "event-like" distribution of interannual peaks (Fig. 3a), which is significantly different from the essentially continuous (Gaussian-type) distribution seen among many of the commonly used ENSO indices, such as NIÑO3.4 and the Southern Oscillation Index (Chiodi and Harrison, 2008, 2010, 2013). This event-like behavior makes the determination of El Niño event-status based on OLR much less ambiguous than when using the commonly used indices (Chiodi and Harrison, 2008).

The interannual peaks seen in the OLR El Niño (minima) and Niño3.4 index (maxima) are plotted against one another in Figure 4a, wherein a dashed line marks the suggested OLR El Niño event threshold of -30 W/m^{-2}. The four large OLR events (red circles) have monthly average OLR peak amplitudes ranging from -24 to -59 $W\ m^{-2}$. The smallest of these, in terms of

OLR, is 0.75 standard deviations removed the next closest (negative) OLR peak seen in the other years. The four large OLR events occur in years with peak monthly-average Niño3.4 values between 1.4 and 2.7 °C. The two years with the strongest SSTAs also have the largest OLR peaks. There are three other years (large red "x") that have Niño3.4 peaks in that exceed 1.4 °C but do not have OLR amplitudes that reach the OLR-event level. Additionally, there are 7 more years (small red "x") that have Niño3.4 peaks within 0.75 standard deviations of 1.4 °C, which is the smallest Niño3.4 peak seen among the four large OLR events. Based on SSTA alone, it is difficult to distinguish these 10 other years (red "x") from the lesser two OLR-event years.

A companion plot of the OLR La Niña index values versus Niño3.4 minima (minimum monthly average seen during the La Niña OLR index integration period) is shown in Figure 4b. In this case, the 6 years identified as OLR La Niña events (OLNI > 30 days; blue circles) have Niño3.4 (negative) peaks in the -0.96 to -2.15°C range. No other years exceed the suggested OLR-event threshold. The spread between the smallest OLNI value seen among the six OLR La Niña years and the nearest non-OLR La Niña year (in terms of OLNI) is 0.5 standard deviations. In the La Niña case, there are 4 years (large blue "x") that have (negative) Niño3.4 peaks < -0.96° C (the smallest SSTA-peak seen among the OLR La Niña events), and another 6 (small red "x") that have Niño3.4 peaks within 0.5 standard deviations of –0.96 °C. Distinguishing the OLR La Niña years from these 10 other years using just SSTA is difficult.

We have also examined the spatial distribution of the SST and SSTAs seen in the commonly identified ENSO years (e.g. Figures 14 and 15 in Appendix A) for indication of their OLR-based categorization. We have not found a way to recover the OLR-identified list of years by considering just tropical Pacific SSTA conditions.

The relationship between the OLR-index and ENSO SSTA behavior can be summarized as follows. The few years with the very largest amplitude SSTAs are generally among those identified by OLR. All years identified by OLR have at least moderately anomalous SSTs (e.g. Niño3.4 amplitudes exceeding 0.85 σ). Yet, several other (non-OLR event) years also have SSTA amplitudes in this (moderate to strong) SSTA range. And there are no discontinuities in the distribution of these SSTAs that correspond to the event-like OLR behavior.

4. Results

4.1. OLR Anomaly Composites

Composite OLR anomalies based on the OLR El Niño years are shown in Figure 5. In each of the seasons considered, taken here as June through August (JJA), September through November (SON), December through February (DJF) and March through May (MAM), a broad and statistically significant negative OLR anomaly (increased atmospheric heating) is seen in the central and eastern tropical Pacific from about the Dateline to 100°W. This anomaly feature strengthens considerably from JJA (Year 0) to DJF (Year 0/1), and maintains much of its amplitude through MAM (Year 1). Also, a statistically significant and positive OLR anomaly is seen in the far Western Pacific that broadens and strengthens during this time. Inspection of the individual years (shown in the Supplementary Material for interested readers) has shown that although there are some differences in OLR anomaly strength among the four OLR El Niño years, especially in the earlier seasons considered, similar anomaly patterns with substantial strength (> 20 W m^{-2}) across the tropical Pacific develop by DJF or MAM in each of these four

years. Thus, significantly anomalous ($p > 0.95$) deep-convection activity across almost the entire tropical Pacific is a robust characteristic of these events.

A different type of behavior is seen in the non-OLR El Niño composite OLR anomalies. In this case, the expanse of the statistically significant and negative anomaly in the eastern central Pacific (160°W to 100°W) is much reduced compared with the OLR El Niño case. And although some positive and statistically significant anomaly is seen in the far western Pacific in JJA and SON, these anomalies weaken in DJF and are no longer apparent by MAM (Fig. 6).

Like the OLR El Niño case, the OLR La Niña composite OLR anomaly patterns are statistically significant across much of the tropical Pacific (Fig. 7). Negative statistically significant anomalies are seen in this case in the far western Pacific whereas positive statistically significant anomalies occur in the near-Dateline region (roughly 150°E to 150°W). Although these patterns can roughly be considered counterparts to oppositely signed features seen in the OLR El Niño composites, upon closer inspection substantial asymmetries are apparent. Notably, in the OLR La Niña events, the positive statistically significant anomalies seen around the Date Line do not reach all the way to the eastern equatorial Pacific. Differences in the seasonal strength of the OLR La Niña and OLR El Niño composites are also evident. Notably, in the OLR La Niña case, the peak amplitudes are seen in SON, whereas in the OLR El Niño case, they occur in DJF.

Okumura and Deser (2010) examined composites of tropical Pacific precipitation anomaly based on El Niño and La Niña years defined using a Niño3.4-based definition (period 1982-2008). They report that the anomaly pattern seen around the end of the calendar year (Year 0/1) in the La Niña case persists longer than that seen in the El Niño case, which, according to

their composites, changes character by boreal spring (i.e. MAM Year 1). A different sort of progression is seen in the OLR El Niño composites shown here. In this case, the DJF (Year 0/1) OLR anomaly pattern maintains amplitude and character through MAM (Year 1). A very different situation, however, is seen in the non-OLR El Niño OLR composites than in the OLR El Niño composites (including oppositely signed anomalies in the eastern Pacific in MAM). The differences in character between our and Okumura and Deser's results likely stem from the fact that their approach mixes, in equal parts, years that are identified by us as both OLR and non-OLR El Niño years.

Examination of the OLR anomalies seen in the six individual OLR La Niña years (shown in the Supplementary Material) has shown that the anomaly pattern seen near the Date Line in SON is a robust feature of these years; each of the six OLR La Niña years had a coherent and substantial (20 to 40 W m^{-2}) positive anomaly in this region in SON. In the subsequent DJF and MAM seasons, however, some years have anomaly amplitudes in the near-Dateline and far western Pacific regions that resemble the pattern but exceed the values seen in SON, whereas others (especially 1974-75) show a different, weaker-amplitude anomaly pattern. Thus, strong mature-stage (DJF and MAM) atmospheric heating anomalies appear to be a possible but not necessarily consistent feature of the OLR La Niña events. On the other hand, strong and consistent forcing during DJF and MAM was seen in each of the OLR El Niño events.

In the non-OLR La Niña case (Fig. 8), coherent and statistically significant OLR anomalies are only seen in both the far western (negative) and near-Date Line (positive) region in the DJF composite. Inspection of the individual years has shown that this feature is not very robust; only three of the six non-OLR La Niña years (1983-84, 1995-96, 2000-01) have DJF anomaly amplitudes greater than 20 W m^{-2} in both the far western and near-Date Line regions.

In the other seasons considered, the composite non-OLR La Niña anomalies in these regions are not nearly as statistically significant as those seen in the OLR La Niña composites.

4.2. Precipitation Anomaly

Precipitation composites based on the OLR El Niño, non-OLR El Niño, OLR La Niña and non-OLR La Niña years are shown in Figures 9-12. In this case, precipitation anomalies are shown where they reach statistical significance at the 80% confidence interval, or better. Comparison with composites masked at higher levels (not shown) suggests that using an 80% cutoff in this case is useful for identifying regions with spatially coherent, if not uniformly significant anomalies. Using a lower confidence interval obviously raises the fraction of the area that can be expected to reach statistical significance misleadingly (i.e. by chance alone). To test whether or not the anomaly patterns we consider are entirely dominated by such results, the global, or "field" (Livezey and Chen, 1983) significance of each composite, based on the extent of the area that reaches local statistical significance, is also estimated by a Monte Carlo approach.

To understand the role of a field significance test in a study such as this, which simultaneously examines many different regions with different types of seasonal weather anomalies, it is important to recognize that some (locally) statistically significant anomaly should be expected even in the case that the results (composite anomaly patterns) are produced by the effects of chance alone (the "null hypothesis"). A field significance test determines, in this case, the amount of locally significant anomaly that must be seen in a composite in order for the null hypothesis to be disproven at the selected confidence interval.

Of the 16 (4 seasons × 4 year lists) seasonal precipitation anomaly composites shown in Figures 9-12, only two are globally (60°N to 60°S), or "field" significant at the 95% level or better; the OLR El Niño DJF composite (Fig. 9) and the OLR La Niña SON composite (Fig. 11).

Many features of the anomaly patterns seen in these composites will be recognizable to readers familiar with the seminal studies of the seasonal weather anomalies associated with ENSO. For example, the locally significant anomalies seen in the SON OLR La Niña composite centered over Uruguay (dry), the Islands of the far western tropical Pacific and Australia (wet), India (wet), Sri Lanka (dry), as well as the anomalies seen in the DJF OLR El Niño composite over southern (dry) and eastern equatorial (wet) Africa, the far western Pacific Island nations and some of Australia (dry), the southern U.S. (wet), northeastern South America (dry) and southern Brazil/Uruguay (wet) are all consistent, at least in a broad sense, with anomalies previously highlighted by the work of Ropelewski and Halpert (1987 and 1989), who examined an earlier period than is considered here [there is only one year of overlap among the 19 La Niña and 25 El Niño years composited by Ropelewski and Halpert and those considered here].

Many of these regional anomalies remain statistically significant in the subsequent seasons (i.e. MAM in the OLR El Niño case; DJF in the La Niña case), which yield precipitation composites that remain globally significant at the 90% level. Such features include the anomalies seen over northeastern South America and Uruguay in the MAM OLR El Niño case. Inspection of the individual years (shown in Supplementary Material) reveals that these features are among the most consistent highlighted by these results. The generally high level of

consistency between the composites discussed here and previously by Ropelewski and Halpert suggests that they are stable features of the influence of ENSO on seasonal weather anomalies.

Other significant anomalies seen in these OLR-identified composites, such as the dry (wet) anomalies seen in SON over the Horn of Africa and Saudi Arabia in the OLR La Niña (El Niño) composite, and the wet anomalies seen over southwestern China in the DJF and MAM OLR El Niño composites (perhaps also the dry anomaly over Thailand in this latter case) were not as prominent in the earlier studies (Ropelewski and Halpert 1987 and 1989, Kiladis and Diaz 1989). And in some instances, statistically significant anomalies are not seen in the OLR-identified composites when and where they may have been expected based just on the seminal studies (e.g. very little statistically significant anomaly is seen over India in the JJA OLR El Niño composite). These differences may be the result of seasonal impacts now better revealed by recent improvements in the observing system, changes in the influence of ENSO, or artifacts of the particular years chosen in this case.

A different type of anomaly pattern is in seen in the precipitation composites based on the non-OLR El Niño and non-OLR La Niña years (Figs. 10 and 12). For example, in SON, when the OLR La Niña case was found to reach peak global significance, there are very few areas in the non-OLR La Niña composite that yield locally significant anomalies, and those that do are characterized by a relatively incoherent mix of positive and negative anomalies. In DJF, when the OLR EL Niño case reached peak global significance, the non-OLR El Niño composite does not yield enough locally significant anomaly to reach global significance at even the 0.50% confidence level (it contains less locally statistically significant anomaly than should be expected based on the effects of randomness alone). With the exception South America, which in the DJF (but not MAM) non-OLR El Niño case resembles a weaker amplitude version of that seen in the

OLR EL Niño composite, it is otherwise difficult to find regions that are statistically significant and have the same sign in both the DJF OLR and non-OLR El Niño composites.

Based on the Monte Carlo methods used here, none of the non-OLR ENSO composites reach field significance at the 90% confidence level. It is notable, however, that the SON non-OLR El Niño composite is not far from being field significant at this level (p=0.84), and has a coherent and statistically significant dry anomaly over most of Australia that may be deserving of further consideration. Interestingly, dry anomaly over most of Australia can also be seen in the preceding JJA non-OLR La Niña composite and inspection of the individual years (see Supplementary Material) reveals that dry anomalies with amplitudes and patterns like those seen in the composites are a relatively consistent (e.g. 5 out of 6) feature of these years, in these seasons. At least over some regions of Australia (e.g. the South and Southwest of Australia in the work of Ropelewski and Halpert, 1987 and 1989; see also the SON results in Kiladis and Diaz 1989) June to November Year 0 El Niño effects on Australian rainfall have also been found previously. The relative lack of dry anomaly over Australia in the OLR EL Niño case at these times raises the possibility that the anomalous tropical Pacific atmospheric heating conditions associated with the non-OLR El Niño years, in which convection is substantially reduced over the far western Pacific and eastern tropical Indian Ocean, but does not increase over the central and eastern tropical Pacific nearly to the extent seen in the OLR El Niño years, may be more conducive to dryness over Australia than the tropical Pacific behavior seen in the OLR El Niño years. Diagnostic modeling, likely with coupled ocean-atmosphere models, which is beyond the scope of this study, will be needed more fully explore the mechanisms responsible.

5. OLR and SSTA based outlooks on ENSO

The OLR indices discussed above are able to identify the tropical Pacific anomaly states most likely to have a meaningful (significant amplitude) and predictable (consistent) influence on global seasonal weather anomalies. The OLR El Niño and OLR La Niña years are typically identified by the end of boreal fall, making their composites directly useful to seasonal forecasting efforts in the ensuing winter and spring seasons. Most of the years in record, however, are not identified as OLR-ENSO years.

In review we were asked if consideration of tropical Pacific OLR behavior can be expected to increase measures of forecast skill based on all years (not just those identified by OLR). To examine this, we have conducted a retrospective forecast (hindcast) experiment in which global precipitation anomaly in the strongly affected DJF season (1974-2011) is hindcast by applying the OLR El Niño and OLR La Niña composites in the years that are identified as such by the OLR El Niño and OLR La Niña indices by the end of fall. Thus, in this "OLR-hindcast", most years have no specified precipitation anomaly, the OLR El Niño composite is applied in the 3 years identified by the OLR El Niño index by the beginning of December and the OLR La Niña composite is applied in 6 years. We compute the anomaly correlation coefficient between the OLR-hindcast and the observed DJF precipitation anomaly over all years, even though non-zero predictions are only made in 9 of the 37 total. The anomaly correlation reaches statistical significance at the 95% level (based on Fisher's "z" methods; see shaded regions in the upper panel of Fig. 13) mainly over the same regions that have statistically significant OLR El Niño and OLR La Niña composite precipitation anomalies (c.f. Figs. 9 and 11). A useful amount of variance is captured by this hindcast in these regions.

For comparison, we also considered a hindcast of DJF precipitation anomaly based on its linear regression with SON-averages of the Niño3.4 index (again using information available by

December Year 0 to forecast DJF conditions). The hindcast anomaly correlation coefficient (again computed over all years) reaches statistical significance at the 95% level over 16% of the land between 60°S and 60°N in this linear-hindcast case (see Fig 13, lower panel), which is about half as much as the 27% that reaches this level of statistical significance in the OLR-hindcast case. Most (75%) of the land area that yields significant correlation in the linear-hindcast case is contained within the regions that do so in the OLR case. In the majority of these regions, the stronger correlation is produced by the OLR-hindcast, which produces a spatially-averaged anomaly correlation of 0.43 over the regions shaded in the upper panel of Fig. 13. We offer this hindcast examination (which assumes a prior knowledge of the OLR-event composites in one case, and the NIÑo3.4-linear-regression coefficient in the other) not as a specific forecasting strategy, but to illustrate that it is beneficial to distinguish the OLR El Niño and OLR La Niña years from others for the purposes of seasonal forecasting in the majority of regions strongly affected by ENSO.

6. Non-linear aspects of the precipitation composites

We are aware that some studies (e.g. Kumar et al. 2007) have suggested, based partly on atmospheric general circulation model experiments, that the influence of ENSO on global atmospheric variability is well represented by a statistical model that predicts atmospheric anomalies based on a linear regression with NIÑO 3.4 SSTA. In other words, that the relationship between NIÑO 3.4 SSTA and atmospheric response is quasi-linear. The composite hindcast results described above suggest that another, more useful, perspective becomes available by looking at OLR. Nonetheless, in the review process, the issue arose of whether such a quasi-linear model (one that posits a linear relationship between NIÑO 3.4 and atmospheric response to ENSO, but also accounts for noise, or sources of atmospheric variability unrelated to

436 ENSO) could be considered consistent with our precipitation composite results. The argument in
437 favor of this being that the OLR identified El Niño and La Niña years have, on average, stronger
438 ENSO SSTA amplitudes than the other non-OLR years. We have examined this question using
439 Monte Carlo methods that simulate land precipitation anomaly in the strongly affected DJF
440 season according to a quasi-linear model based on the "signal-to-noise" measure used by Kumar
441 et al. (2007), who also considered DJF.

442 The Northern Hemisphere winter (e.g. DJF) is the time of year during which ENSO
443 events typically peak in the tropical Pacific. It is also when many of the statistical linkages
444 between ENSO-state and seasonal weather anomalies elsewhere are at, or near, their strongest.
445 The global land precipitation composites based on the OLR-identified subsets of El Niño and La
446 Niña years each reach field significance during DJF based on the amount of locally statistically
447 significant anomaly contained in them (at the 90% and 95% levels, respectively). By the same
448 measure, however, the non-OLR El Niño and non-OLR La Niña precipitation composites are
449 indistinguishable from randomness at this time (they contain amounts of locally statistically
450 significant anomaly that rank at the 41st and 47th percentile, respectively; in other words, slightly
451 less than the amount expected on based on pure random selection, which is 50%).

452 To test whether these observational results are consistent with the quasi-linear model, we
453 follow the methods of Kumar et al. (2007) in computing a signal-to-noise ratio based on a linear
454 regression between DJF-averaged precipitation anomaly and DJF-averaged NIÑO3.4 SSTA. In
455 this case the "signal" is the amount of observed precipitation variability that is linearly related to
456 the NIÑO3.4 index, and the "noise" is the remainder. These terms are determined at each land
457 location by calculating the regression coefficient (c) in the following linear-model,

458 $$p'(t) = c * NIÑO3.4(t) + n(t). \quad \text{Eqn. (1)}$$

459 Here *p'(t)* is the precipitation anomaly averaged over DJF of year *t*, and *c* is defined at each land
460 location based on least-squares methods. The signal-to-noise ratio, then, is the standard
461 deviation of the *c*NIÑO3.4(t)* term computed over the 37 DJFs in the study period divided by
462 the standard deviation of *n(t)* over that same time.

463 The DJF precipitation anomaly signal-to-noise ratio thus defined is shown in Appendix
464 B, for reference (Figure 16). Comparison with Figures 9 and 11 reveals that the strongest signal-
465 to-noise ratios are found mainly in the same regions that have statistically significant anomalies
466 in the OLR El Niño and OLR La Niña composites.

467 We use Monte Carlo methods to test whether or not this linear model is consistent with
468 the observed variability. Specifically, we examine whether or not the model can easily
469 reproduce precipitation composites that in one case (based on the OLR-identified subset of
470 years) reach field significance at standard confidence intervals, while the other (based on the
471 non-OLR subset of years) are indistinguishable from randomness.

472 To proceed, we need to decide how many land locations should be resolved in the
473 simulation. Since the precipitation time series at each grid point in a data set like the one we
474 consider should not generally be considered to vary independently from those surrounding it, a
475 first step here involves estimating the effective number of spatial degrees of freedom (ESDOF)
476 contained in the GPCC land precipitation data. We have done this based on the methods of
477 Bretherton et al. (1999), as described in Appendix B, and found that a range, rather than specific
478 number of ESDOF is suggested by this approach. We have therefore repeated the simulation
479 over an extended range of ESDOF (25 to 200).

480 To simulate the land precipitation anomaly, the *c*NIÑO3.4(t)* time series is specified as
481 the "signal" at each land location. The signal stays fixed during the simulation. A different
482 independently selected noise term, which we select from a random normal distribution with
483 standard deviation chosen to match the ratio shown in Fig. 1, is then added to the signal in each
484 iteration. We have confirmed that the observed "noise" terms do not generally violate the classic
485 Kolmogorov-Smirnov test for normality, suggesting that the use of a random a normal
486 distribution is appropriate in this case. The simulated data is then tested for field significance
487 (after each iteration) following the procedure described in the main text and used for the
488 observations.

489

490 We find that the simulation's quantitative behavior depends on the ESDOF used, but
491 even in the most lenient scenario (lowest ESDOF), it is at least "unlikely" (Mastrandrea, 2010)
492 that the quasi-linear model yields a non-OLR La Niña (El Niño) global land precipitation
493 anomaly composite that contains as little, or less, statistically significant anomaly as is seen in
494 the observations (see Table 2). In other words, the linear model usually predicts that a stronger
495 response (more statistically significant anomaly) should be seen in the non-OLR composites than
496 is actually observed. And if the initial estimates of ESDOF are conservative, as we expect, then
497 it is at least "very unlikely", and quite possibly "exceptionally unlikely" that the quasi-linear
498 model is consistent with the observed variability in this respect. Under these assumptions, the
499 linear-model almost always predicts that the non-OLR precipitation composites would also be at
500 least moderately field significant (in addition to the OLR event composites).

501

The results of this section can be summarized as follows. Depending on the ESDOF assumed, it is "unlikely" to "exceptionally unlikely" that the quasi-linear relationship of Kumar et al. (2007) can explain our composite results, which find strong and robust precipitation anomaly patterns in the DJF OLR El Niño and OLR La Niña composites, but composites that are indistinguishable from noise based on the other non-OLR ENSO years. The quasi-linear model fails because, given the strength and consistency of the of the precipitation anomaly patterns in the OLR-identified events, the quasi-linear model predicts that more statistically significant anomaly should be seen in the other years (non-OLR years) than is actually seen in the observations.

These results support our conclusion that it is useful to pay attention to OLR for the purposes of identifying the years that are most likely to exhibit the seasonal weather anomaly patterns that have traditionally been associated with El Niño and La Niña extremes.

7. Summary and Discussion

It is well known that there is generally large event to event variability in seasonal precipitation anomaly patterns associated with El Niño and La Niña events defined by their NIÑO3.4 values. While the familiar seasonal precipitation anomaly patterns are not strongly affected by the details of the lists of years that go into them, many individual years indentified based on SST will not exhibit the composite patterns. We have shown here that taking an OLR perspective to identify subsets of El Niño and La Niña events, which we call "OLR-El Niño" and "OLR-La Niña" events, offers a way to identify highly statistically significant regional precipitation anomalies and that many of these patterns are quite robust from year to year. Evidently the OLR-event years have a stronger connection to the processes that control precipitation anomalies.

The OLR-event years are distinguished by OLR-index values that attain a rather clear separation (> 0.5 standard deviations) from the background variability seen at other times. There is no simple way to recover the OLR-event perspective by looking at ENSO SSTA; no similar separation is seen in NIÑO3.4 SSTA (which follows a continuous distribution), and some of the years with the strongest ENSO SSTAs are not among those identified as OLR-events. Strong SSTA appears to be a necessary, but not sufficient condition for these OLR-events.

To identify the OLR events we have made use of indices constructed from OLR observations, which have been available from the mid-1970s. We have used the OLR-El Niño index of Chiodi and Harrison (2013) which is based on monthly average conditions over the eastern central equatorial Pacific, and which usefully identifies when deep convection has moved further eastward into the Cold Tongue than normal. To identify the OLR-La Niña events we have introduced a new index that counts the number of nearly clear-sky days in the heart of the normal region of deep equatorial atmospheric convection. The latter index is usefully more skillful for our purposes than any other we have considered. We present seasonal precipitation anomaly composites, masked for statistical significance over the four OLR-El Niño years and separately over the six OLR-La Niña years. Further, we show how similar are the patterns year-by-year within each composite (see Supplemental Material). These results extend the work of Chiodi and Harrison (2013), which considered El Niño-related seasonal weather anomalies over the contiguous U.S., to global seasonal precipitation anomalies.

Precipitation anomalies that are globally ("field") significant at the 90% confidence interval (or better) are identified in the wintertime (DJF Year 0/1) OLR La Niña composite, as well as in the wintertime OLR El Niño composite. All six years in the OLR La Niña composite as well as 3 of the 4 years in the OLR El Niño composite are identified by the respective OLR

indices in time to be of use to wintertime and later seasonal forecasting efforts. To the extent the behavior seen in the study period continues, these indices will provide a useful indicator for the impacts of these events on wintertime precipitation anomaly even without longer lead forecasts of tropical Pacific OLR behavior.

Globally significant precipitation anomaly is seen at the 90% level in the spring (MAM Year 1) OLR El Niño composite as well. The OLR El Niño index therefore also does not require longer-lead forecasts of OLR in order to be a useful indicator for the impacts of OLR El Niño events on springtime precipitation.

Globally significant precipitation anomaly is also seen at the 90% level in the fall (SON Year 0) OLR La Niña and OLR El Niño composites. The OLR La Niña and OLR El Niño indices therefore would require longer-lead forecasts of OLR in order to be useful indicators for the impacts of OLR La Niña and OLR El Niño events on fall precipitation. The prospects for doing this deserve further study.

In addition to the OLR-identified years, the NOAA historical definition based on five consecutive months of the 3-month running average Niño 3.4 SSTA >0.5°C or <-0.5°C, gives ENSO-status to several others in the study period that are not identified based on OLR. Although consistent precipitation anomaly patterns are seen in the far western Pacific and over Australia in the JJA and SON non-OLR El Niño composites (suggesting this area as one in need of further study for regional mechanistic understanding and forecast effectiveness), our results do not support widespread influence of these non-OLR ENSO years on global precipitation anomaly patterns. In most areas, the non-OLR years, on average, do not exhibit statistically useful precipitation anomaly patters.

569 Based on the Monte Carlo method used, none of the non-OLR precipitation composites
570 reach field significance at the 90% level or better. Notably, in contrast to both the DJF OLR El
571 Niño and DJF OLR La Niña cases, the non-OLR DJF composites even fail to show the amounts
572 of locally statistically significant precipitation anomaly that should be expected based on the
573 effects of chance (random selection of years) alone. It is difficult to rationalize this difference
574 between the OLR and non-OLR global precipitation composites by assuming that a linear
575 relationship exists between global precipitation anomaly and ENSO SSTAs. If there is a
576 statistically useful linkage between these other events and seasonal precipitation anomaly, it is
577 over significantly fewer regions than seen in the OLR El Niño and OLR La Niña cases.

578 This work strongly suggests that there are immediately realizable benefits to using OLR
579 behavior to identify the tropical Pacific events that are most likely influence seasonal weather
580 anomalies on a global scale. Notably, our OLR-based indices offer a method for clearly
581 detecting, in what is currently a subset of the commonly identified ENSO years, when increased
582 levels of confidence can be placed in DJF and later ENSO-type seasonal forecasts.

583 Our results apply to the majority of the regions strongly affected by ENSO. However,
584 when interest is in a specific region, it is always prudent to carefully consider as much of the
585 relevant and available information as possible. We must leave it to the forecasting community to
586 decide how best to employ our results to further specific national forecast objectives.

587 The mechanisms responsible for the different behavior of SSTA and OLR based indices,
588 and the global weather anomalies associated with ENSO events merits additional research. As
589 forecast skill for OLR conditions improves we may anticipate longer-lead skillful ENSO
590 seasonal weather anomaly forecasts in many regions.

591

592

593

594 Appendix A: Tropical Pacific SSTAs

595 The 3-month average tropical Pacific SSTAs seen during September through November
596 (Year 0) of the years with ENSO status based on the NOAA definition are shown in this
597 appendix for reference. The years identified as El Niño by the NOAA (SSTA-based) definition
598 are shown in Figure 15, and the La Niña years in figure 16. The OLR indices for ENSO
599 discussed herein identify the OLR-ENSO events by the beginning of December (Year 0) in 9 of
600 10 cases.

601

602 Appendix B: Estimating the effective number of spatial degrees of freedom
603 (ESDOF)

604

605 To estimate the ESDOF contained in DJF averaged land precipitation anomaly (period 1975-
606 2011), we referred to the two methods discussed by Bretherton et al. (1999). Computing
607 ESDOF over each continent (see boxes in Fig. 16), we find 53 and 70 total ESDOF based on the
608 "mixed-moment" and "eigenvalue formula" methods, respectively. Bretherton et al. (1999)
609 reports that when the number of sampling times are less than a few hundred and not much
610 greater than the ESDOF (as is the case here), the mixed moment approach is unstable (exhibits

large scatter) and the eigenvalue-formula approach tends to be biased low. This suggests that these estimates are conservative. Further examination has shown that when the ESDOF is computed over smaller regions and summed, larger sums are produced. For example, we find that the eigenvalue-formula yields 112, rather than 70 ESDOF, when the total ESDOF is estimated based on considering the tropical and non-tropical regions of the larger continents separately. It appears to be hard to be precise about the ESDOF contained. Thus, we have computed results over an extended range of possibilities (25 to 200 ESDOF).

Acknowledgments: This publication is [partially] funded by the Joint Institute for the Study of the Atmosphere and Ocean (JISAO) under NOAA Cooperative Agreement NA10OAR4320148, and by support from the Climate Observations Division of the NOAA Climate Program Office as well as from NOAA's Pacific Marine Environmental Laboratory. This is JISAO Contribution No. 2068, and NOAA Pacific Marine Environmental Laboratory Contribution No. 3946.

630 References:

631 Chiodi, A.M., and D.E. Harrison, 2008: Characterizing the interannual variability of the
632 equatorial Pacific: An OLR perspective. NOAA Tech. Memo. OAR PMEL-140, NTIS:
633 PB2008-112890, Seattle, WA, 30 pp.

634 Chiodi, A.M., and D.E. Harrison, 2010: Characterizing warm-ENSO variability in the equatorial
635 Pacific: An OLR perspective. *J. Climate*, **23**, 2428–2439.

636 Chiodi, A.M., and D.E. Harrison, 2013: El Niño impacts on seasonal U.S. atmospheric
637 circulation, temperature and precipitation anomalies: The OLR-event perspective. *J.*
638 *Climate*, doi: 10.1175/JCLI-D-12-00097.1. [in press]

639 Bretherton, C. S., M. Widmann, V. P. Dymnikov, J. M. Wallace and I. Blade, 1999: The
640 Effective Number of Spatial Degrees of Freedom of a Time-Varying Field. *J. Climate*,
641 **12**, 1990-2009.

642 Ephron, *B., and R.* Tibshirani, *1991: Statistical Data Analysis in the Computer Age*, *Science*,
643 **253**, 390-395.

644 Garreaud, R. D. and J. M. Wallace, 1997: Summertime incursions of Midlatitude air into
645 subtropical and tropical South America. *Mon. Wea. Rev.* , **126**, 2713-2733.

646 Garreaud, R. D., and D. S. Battisti, 1999: Interannual ENSO and interdecadal ENSO-like
647 variability of the tropospheric circulation in the Southern Hemisphere. *J. Climate*, **12,**
648 2113–2123.

649 Halpert, M. S. and C. F. Ropelewski, 1992: Surface temperature patterns associated with the
650 Southern Oscillation, *J. Climate*, **5**, 577-593.

651 Harrison, D.E., and N.K. Larkin, 1998: Seasonal U.S. temperature and precipitation anomalies
652 associated with El Niño: Historical results and comparison with 1997–1998. *Geophys.*
653 *Res. Lett*., **25**(21), 3959–3962.

654 Hoerling, M.P., A. Kumar and M. Zhong, 1997: El Niño, La Niña, and the Nonlinearity of Their
655 Teleconnections. *J. Climate*, **10**, 1769-1786.

656 Hoerling, M.P. and A. Kumar, 2002: Atmospheric Response Patterns Associated with Tropical
657 Forcing. *J. Climate*, **15**, 2184-2203.

658 Horel, J. D. and J. M. Wallace, 1981: Planetary-Scale Atmospheric Phenomena Associated with
659 the Southern Oscillation. *Mon. Wea. Rev.,* **109**, 813-829.

660 Kalnay et al.,1996: The NCEP/NCAR 40-year reanalysis project, *Bull. Amer. Meteor. Soc*., **77**,
661 437-470.

662 Kumar, A., B. Jha, Q. Zhang, and L. Bounoua, 2007: A New Methodology for Estimating the
663 Unpredictable Component of Seasonal Atmoshperic Variability. *J. Climate*, **20**, 3888-
664 3901.

665 Larkin, N.K., and D.E. Harrison (2002): ENSO warm (El Niño) and cold (La Niña) event life
666 cycles: Ocean surface anomaly patterns, their symmetries, asymmetries, and implications.
667 J. Climate, 15(10), 1118–1140.

668 Larkin, N.K. and D.E. Harrison, 2005: Global seasonal temperature and precipitation anomalies
669 during El Niño autumn and winter. *Geophys. Res. Lett.,* **32**, L16705, doi:
670 10.1029/2005GL022860.

671 -- and -- (2005): On the definition of El Niño and associated seasonal average U.S. weather
672 anomalies. *Geophys. Res. Lett*., **32**(13), L13705, doi: 10.1024/2005GL022738.

673 Liebmann B. and C.A. Smith, 1996: Description of a Complete (Interpolated) Outgoing
674 Longwave Radiation Dataset. *Bull. Amer. Met. Soc*., **77**, 1275--1277.

675 Livezey, R. E., and W. Y. Chen, 1983: Statistical field significance and its determination by
676 Monte Carlo techniques. *Mon. Wea. Rev.*, **111,** 46–59.

677 Mastrandrea, M.D., C.B. Field, T.F. Stocker, O. Edenhofer, K.L. Ebi, D.J. Frame, H. Held, E.
678 Kriegler, K.J. Mach, P.R. Matschoss, G.-K. Plattner, G.W. Yohe, and F.W. Zwiers, 2010:
679 Guidance Note for Lead Authors of the IPCC Fifth Assessment Report on Consistent
680 Treatment of Uncertainties. Intergovernmental Panel on Climate Change (IPCC).

681 Okumura, Y. M. and C. Deser, 2010: Asymmetry in the Duration of El Niño and La Niña. *J.*
682 *Climate*, **23**, 5826-5843.

683 Peng, P., and A. Kumar, 2005: A large ensemble analysis of the influence of tropical SSTs on
684 seasonal atmospheric variability. *J. Climate,* **18,** 1068–1085.

685 Rasmusson, E. M., and T. H. Carpenter 1982: Variations in tropical sea surface temperature and
686 surface wind fields associated with the Southern Oscillation/El Niño, *Mon. Wea. Rev.*,
687 **110,** 354–384.

688 Rayner, N. A.; Parker, D. E.; Horton, E. B.; Folland, C. K.; Alexander, L. V.; Rowell, D. P.;
689 Kent, E. C.; Kaplan, A. (2003) Global analyses of sea surface temperature, sea ice, and
690 night marine air temperature since the late nineteenth century, *J. Geophys. Res.*, **Vol. 108**,
691 No. D14, 4407 10.1029/2002JD002670

692 Ropelewski, C.F. and M. S. Halpert, 1986: North American precipitation and temperature
693 patterns associated with the El Niño Southern Oscillation (ENSO), *Mon. Wea. Rev*, **114**,
694 2352-2362.

695 Ropelewski, C.F. and M. S. Halpert, 1987: Global and Regional Scale Precipitation Patterns
696 Associated with the El Niño/Southern Oscillation, Mon. Wea. Rev, 115, 1606-1626.

697 Ropelewski, C.F. and M. S. Halpert, 1989: Precipitation Patterns Associated with the high index
698 phase of the Southern Oscillation, *Mon. Wea. Rev*, **115**, 1606-1626.

699 Rudolf, B., et al. (2010): GPCC Status Report December 2010 (On the most recent gridded
700 global data set issued in fall 2010 by the Global Precipitation Climatology Centre
701 (GPCC))

702 Rudolf, B., U. Schneider (2005): Calculation of Gridded Precipitation Data for the Global Land-
703 Surface using in-situ Gauge Observations, Proceedings of the 2nd Workshop of the
704 International Precipitation Working Group IPWG, Monterey October 2004,
705 EUMETSAT, ISBN 92-9110-070-6, ISSN 1727-432X, 231-247.

706 Smith, S. R., D. M. Legler, M. J. Remigio and J. J. O'Brien, 1999: Comparison of 1997-98 U.S.
707 temperature and precipitation anomalies to historical ENSO warm phases, *J. Climate*,
708 **12**, 3507-3515.

709 Trenberth, K. E., G. W. Branstator, D. Karoly, A. Kumar, N-C. Lau, and C. Ropelewski, 1998:
710 Progress during TOGA in understanding and modeling global teleconnections associated
711 with tropical sea surface temperatures, *J. Geophys. Res*., **103**, 1429114324.

712 Wolter, K., R. M. Dole, and C. A. Smith, 1999: Short-term climate extremes over the continental
713 United States and ENSO. Part I: Seasonal temperatures. J. Climate, **12**, 3255-3272.

714
715
716
717
718
719
720
721
722
723
724
725
726
727
728
729
730
731
732

Tables:

ENSO-Year	1974-75	1975-76	1988-89	1998-99	1999-2000	2010-11
Date	Sep 1974	Jul 1975	Sep 1988	Nov 1998	Oct 1999	Sep 2010

Table 1: Dates on which the OLR La Niña index initially crossed the 30-day threshold.

ESDOF	25	50	75	100	125	200
Non-OLR La Niña	19%	12%	9%	6%	4%	0.2%
Non-OLR El Niño	18%	14%	10%	6%	5%	0.3%

Table 2. Chance that the Mont-Carlo simulation (based on linear-regression with NIÑO3.4) reproduces a non-OLR ENSO year precipitation composite with as little, or less, statistically significant anomaly as is seen in the observations.

750 Figure Captions.

751 Figure 1. The familiar ENSO cartoons, illustrating the subsurface (thermocline) surface (SSTA,
752 SLP, near surface winds) and atmospheric convection conditions commonly associated with the
753 La Niña, ENSO-neutral (middle panel) and El Niño state.

754 Figure 2. Long-term averaged change in OLR between La Niña minus ENSO-neutral
755 conditions. To produce this figure, ENSO anomaly states were defined using a preliminary
756 0.75°C Niño3.4 SSTA threshold (e.g. ENSO-neutral here defined as all times with |Niño 3.4
757 SSTA| < 0.75°C.

758 Figure 3: a) The Chiodi and Harrison (2013) OLR EL Niño index, b) the OLR La Niña index and
759 c) NIÑO3.4 region SSTA.

760 Figure 4. Upper panel: Minimum monthly average OLR El Niño Index versus maximum
761 monthly average Niño 3.4 SSTA seen each year (July to June 1974/75-2010/11). Lower Panel:
762 OLR La Niña index (OLNI) versus minimum monthly average Niño 3.4 SSTA seen during the
763 OLNI integration period. In each panel, the OLR-index values lying between the weakest event
764 and closest non-event are shaded. The equivalent distance (in standard deviations) behind the
765 weakest-event-SSTA peak is also shaded for reference.

766 Figure 5: OLR El Niño event composite OLR anomaly. The anomaly is shaded where
767 amplitudes are significant at the 95% confidence level.

768 Figure 6: Non-OLR El Niño event composite OLR anomaly. The anomaly is shaded where
769 amplitudes are significant at the 95% confidence level.

Figure 7: OLR La Niña event composite OLR anomaly. The anomaly is shaded where amplitudes are significant at the 95% confidence level.

Figure 8: Non-OLR La Niña event composite OLR anomaly. The anomaly is shaded where amplitudes are significant at the 95% confidence level.

Figure 9: OLR El Niño event composite precipitation anomaly. Shading where amplitudes are significant locally at the 80% confidence level. Field significance listed in red.

Figure 10: The non-OLR El Niño event composite precipitation anomaly. Shading where amplitudes are significant locally at the 80% confidence level. Field significance listed in red.

Figure 11: The OLR La Niña event composite precipitation anomaly. Shading where amplitudes are significant locally at the 80% confidence level. Field significance listed in red.

Figure 12: The non-OLR La Niña event composite precipitation anomaly. Shading where amplitudes are significant locally at the 80% confidence level. Field significance listed in red.

Figure 13. DJF precipitation anomaly hindcast results. Period 1974-2011. Upper panel: Shading where OLR-hindcast anomaly correlation is statistically significant at the 95% level. 27% of the land is shaded. In the OLR-hindcast, finite (non-zero) anomalies are only specified in the hindcast in the 9 years identified by the OLR indices prior to boreal winter. The anomaly correlation, however, is computed over all years. Lower panel: Shading where the linear-regression hindcast anomaly correlation is statistically significant at the 95% level. In this case, only 16% of the land is shaded, even though finite anomalies are specified in each year.

Figure 14. SON-averaged SSTA in the tropical Pacific in the years with El Niño status based on the NOAA Historical ENSO definition (1974-2011).

Figure 15. SON-averaged SSTA in the tropical Pacific in the years with La Niña status based on the NOAA Historical ENSO definition (1974-2011).

Figure 16. The "signal-to-noise" ratio for DJF-averaged land precipitation anomaly based on a linear regression with DJF-averaged NIÑO3.4 SSTA.

Figures.

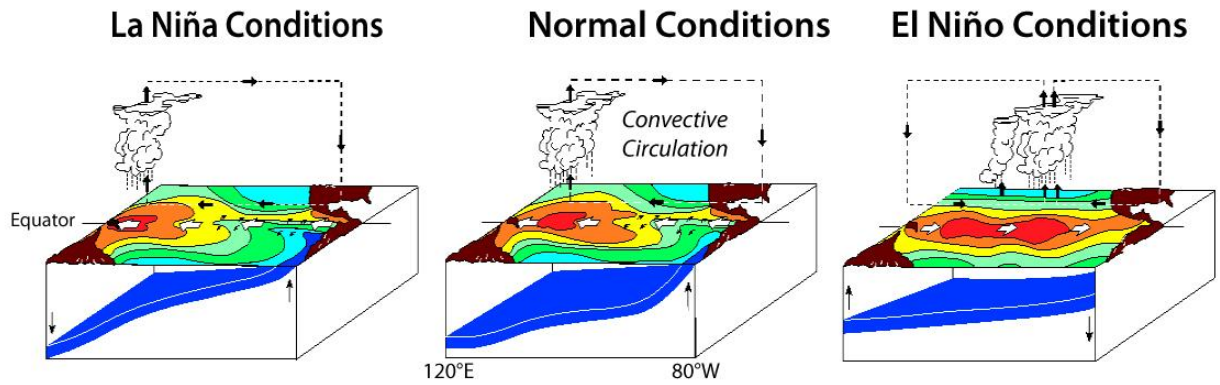

Figure 1. The familiar ENSO cartoons, illustrating the subsurface (thermocline) surface (SSTA, SLP, near surface winds) and atmospheric convection conditions commonly associated with the La Niña, ENSO-neutral (middle panel) and El Niño state.

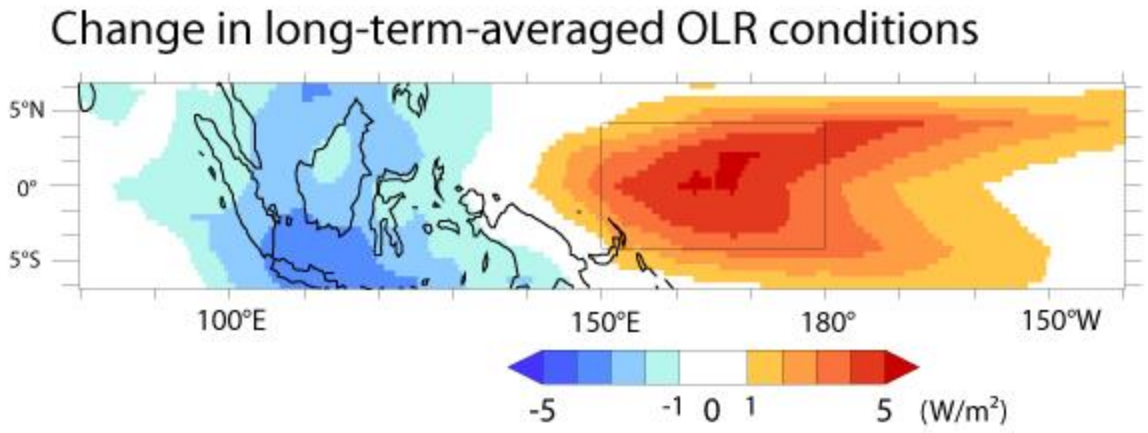

827

828 Figure 2. Long-term averaged change in OLR between La Niña minus ENSO-neutral

829 conditions. To produce this figure, ENSO anomaly states were defined using a preliminary

830 0.75°C Niño3.4 SSTA threshold (e.g. ENSO-neutral here defined as all times with |Niño 3.4

831 SSTA| < 0.75°C.

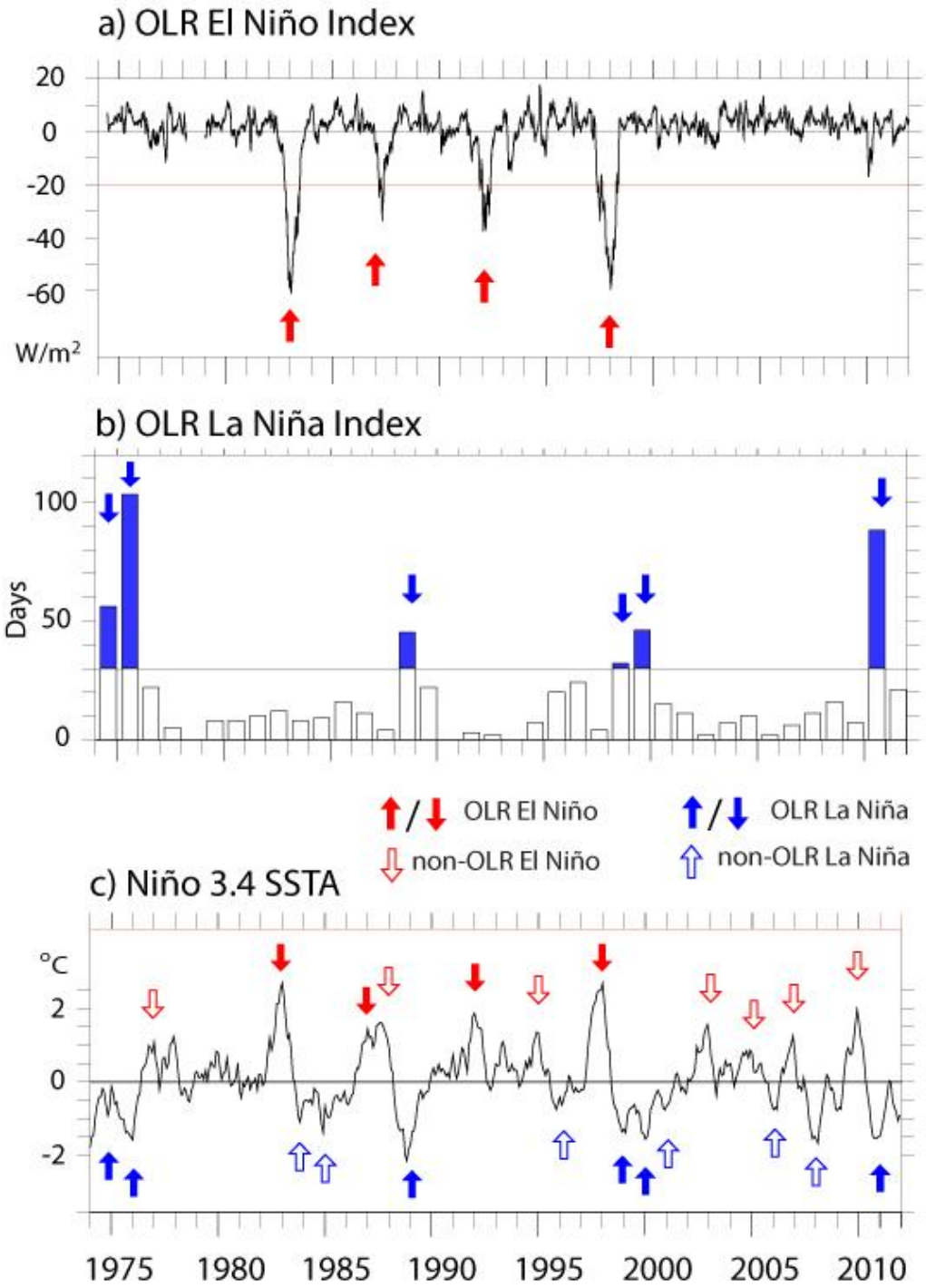

832

833 Figure 3: a) The Chiodi and Harrison (2013) OLR EL Niño index, b) the OLR La Niña index and

834 c) NIÑO3.4 region SSTA.

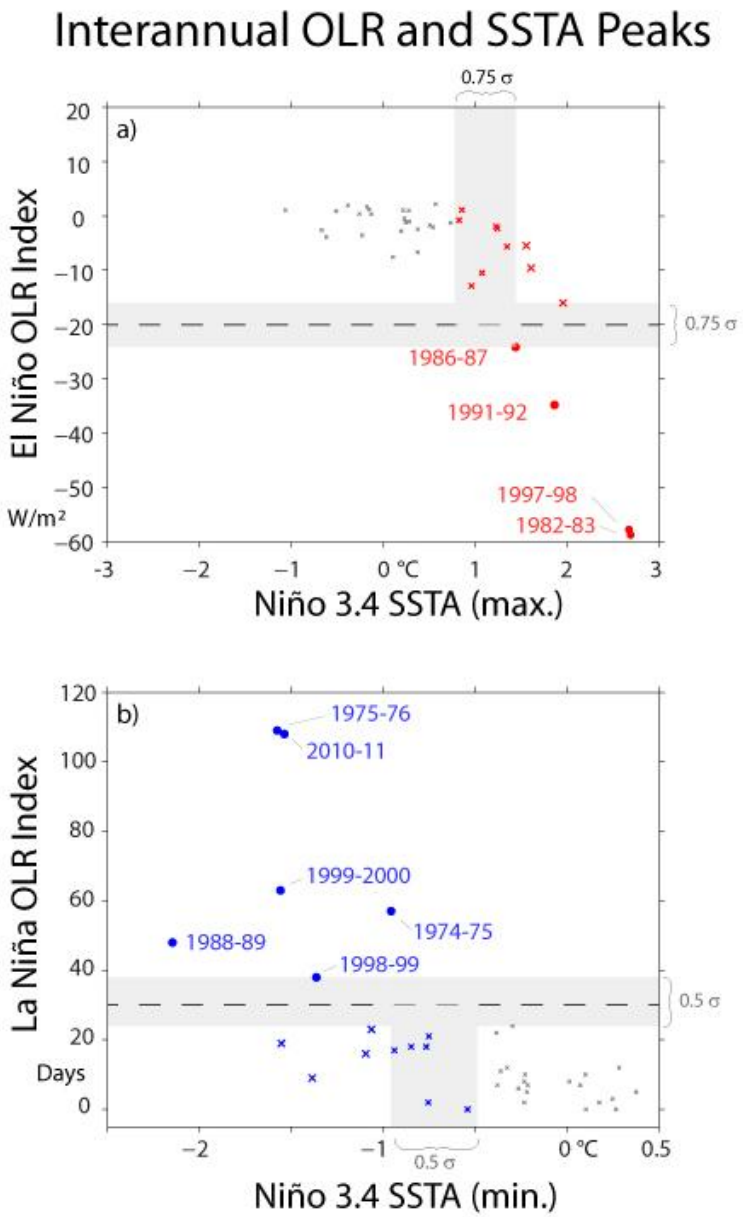

Figure 4. Upper panel: Minimum monthly average OLR El Niño Index versus maximum monthly average Niño 3.4 SSTA seen each year (July to June 1974/75-2010/11). Lower Panel: OLR La Niña index (OLNI) versus minimum monthly average Niño 3.4 SSTA seen during the OLNI integration period. In each panel, the OLR-index values lying between the weakest event and closest non-event are shaded. The equivalent distance (in standard deviations) behind the weakest-event-SSTA peak is also shaded for reference.

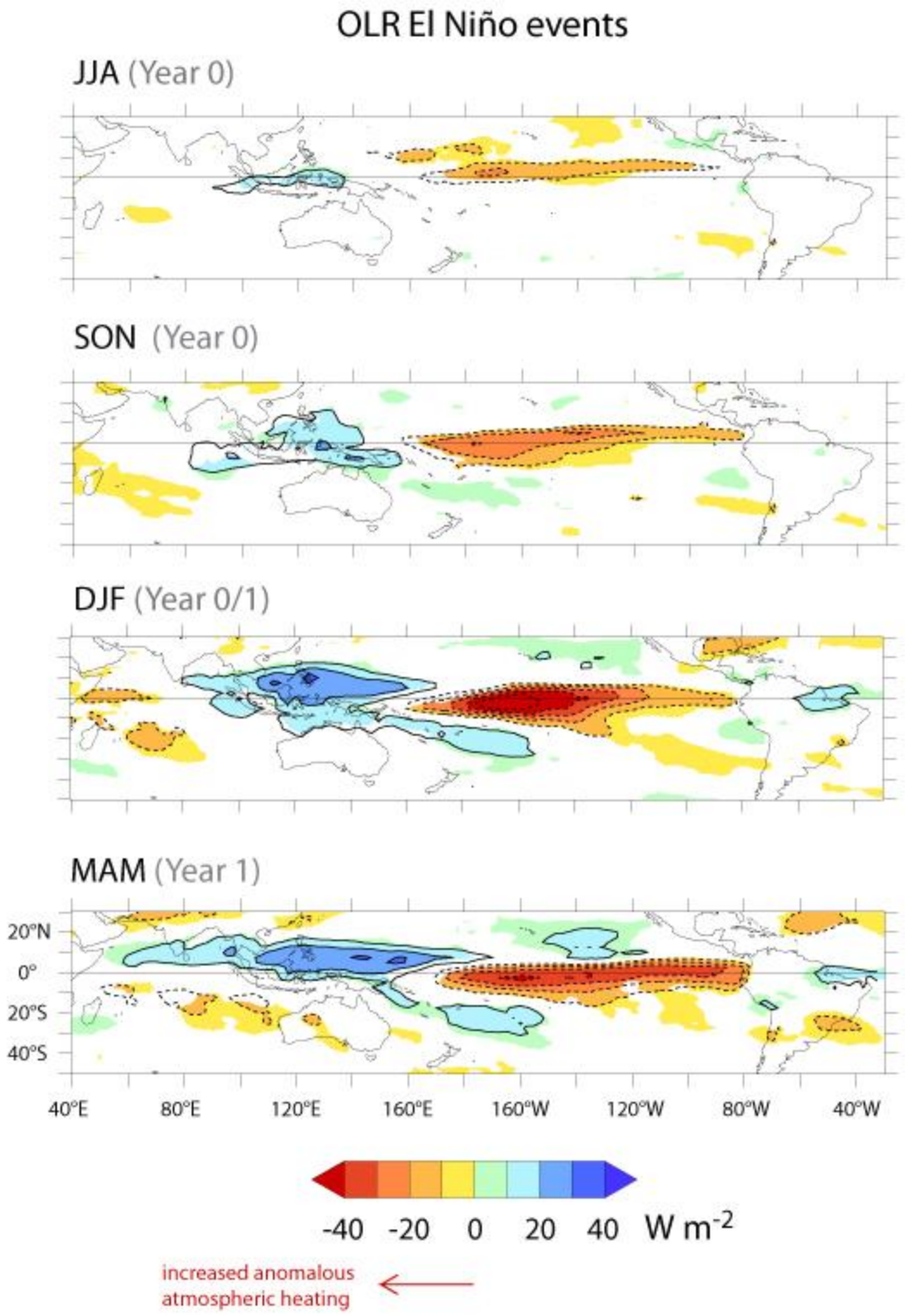

842

843 Figure 5: OLR El Niño event composite OLR anomaly. The anomaly is shaded where

844 amplitudes are significant at the 95% confidence level.

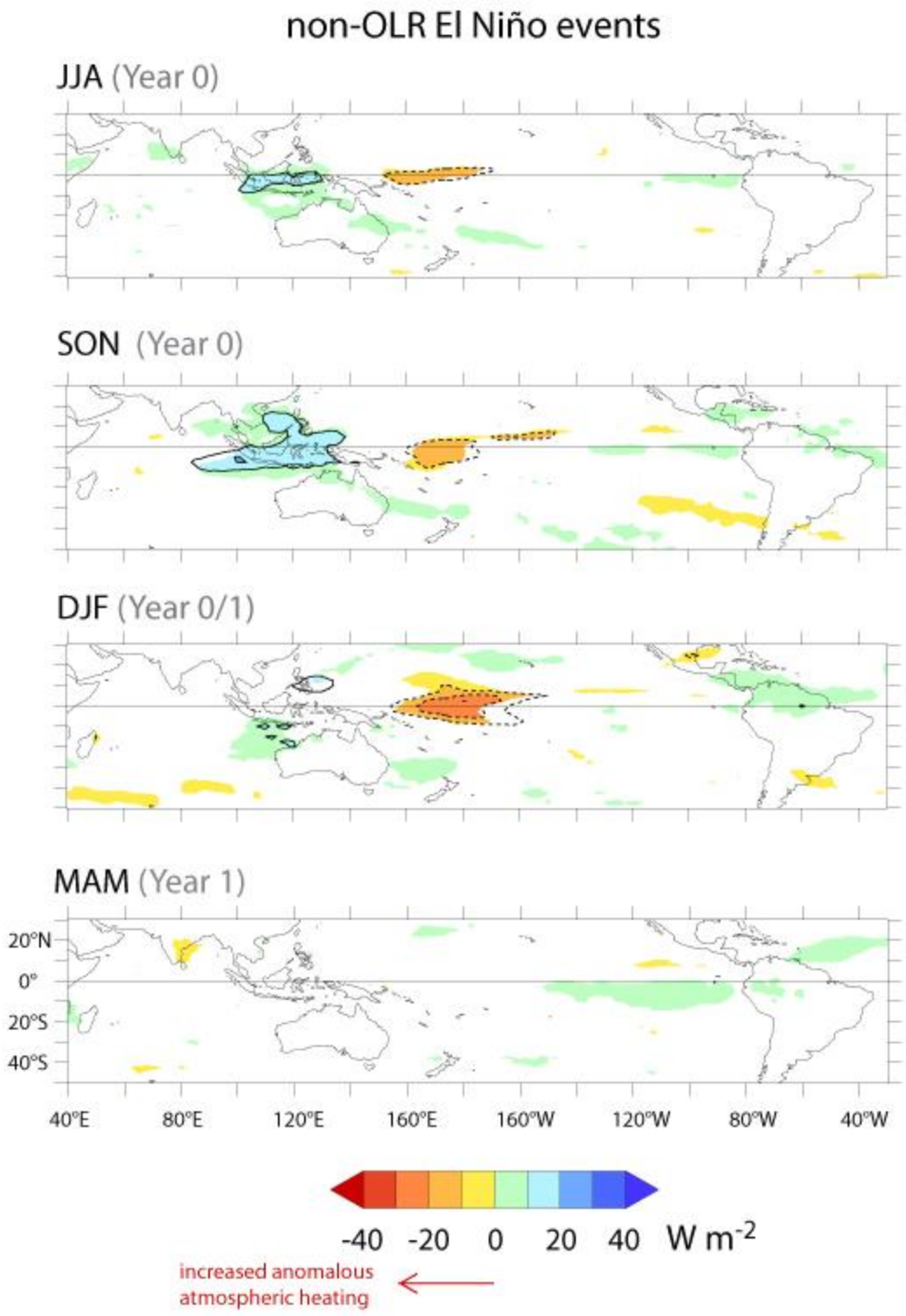

Figure 6: Non-OLR El Niño event composite OLR anomaly. The anomaly is shaded where amplitudes are significant at the 95% confidence level.

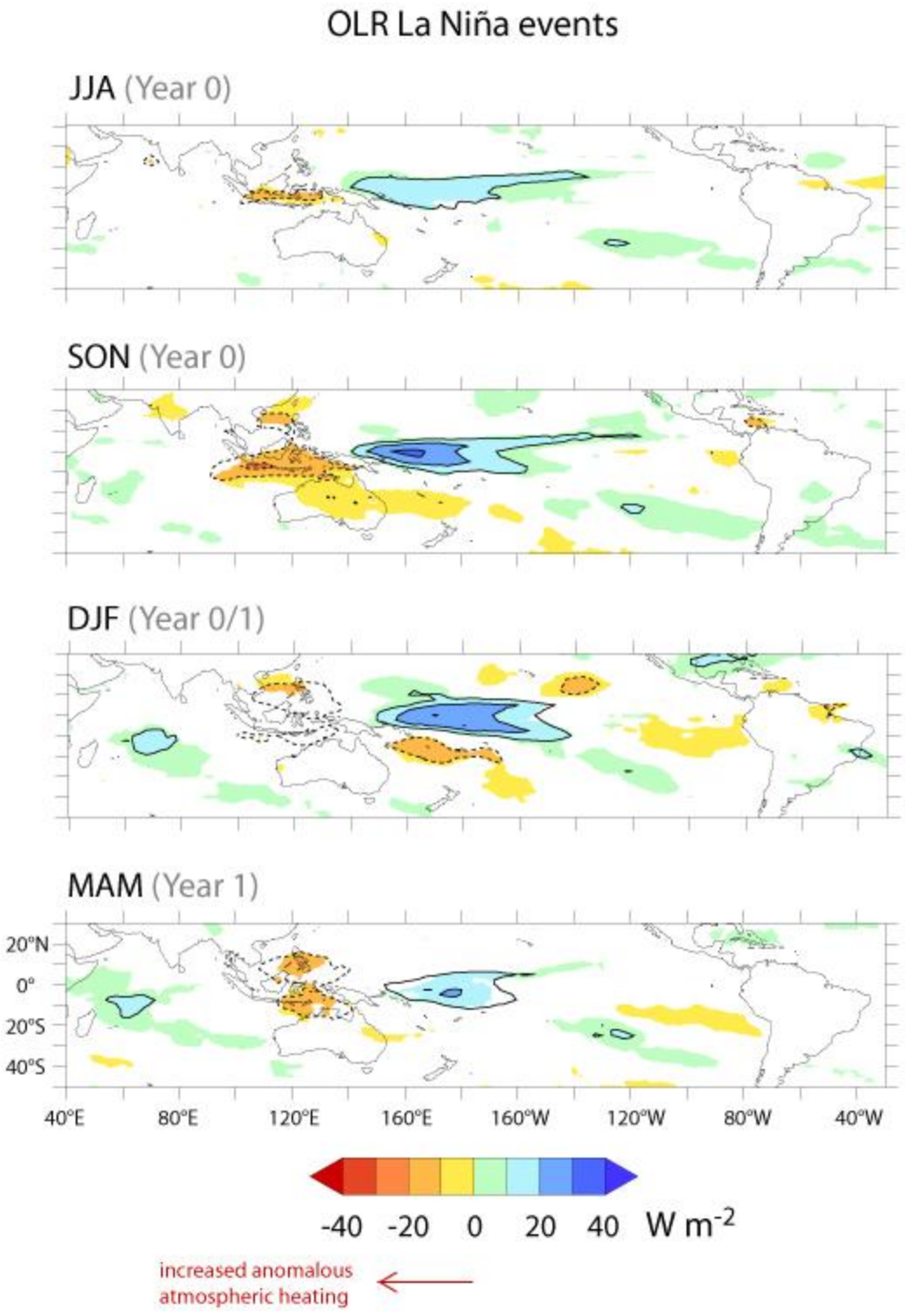

Figure 7: OLR La Niña event composite OLR anomaly. The anomaly is shaded where amplitudes are significant at the 95% confidence level.

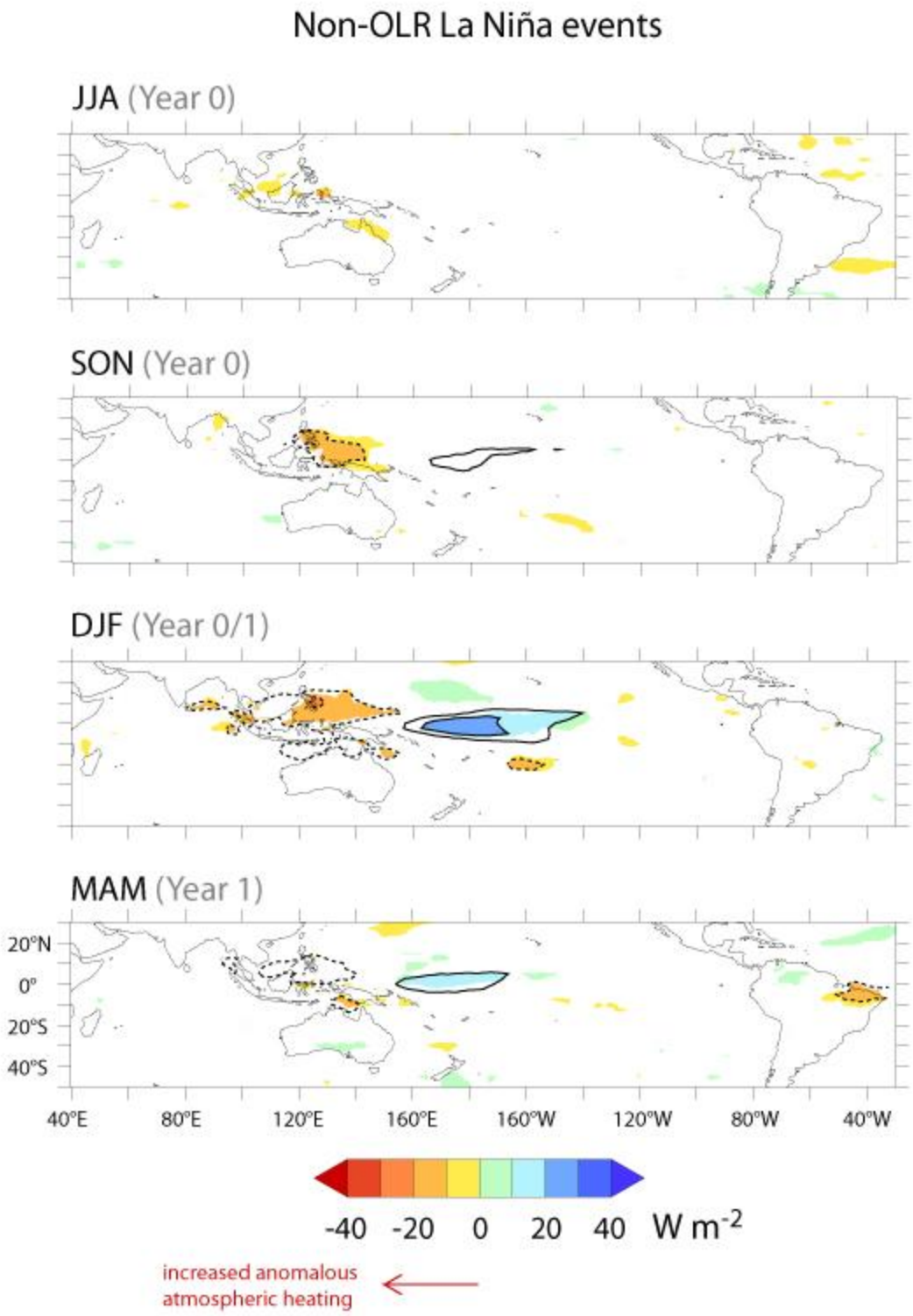

Figure 8: Non-OLR La Niña event composite OLR anomaly. The anomaly is shaded where amplitudes are significant at the 95% confidence level.

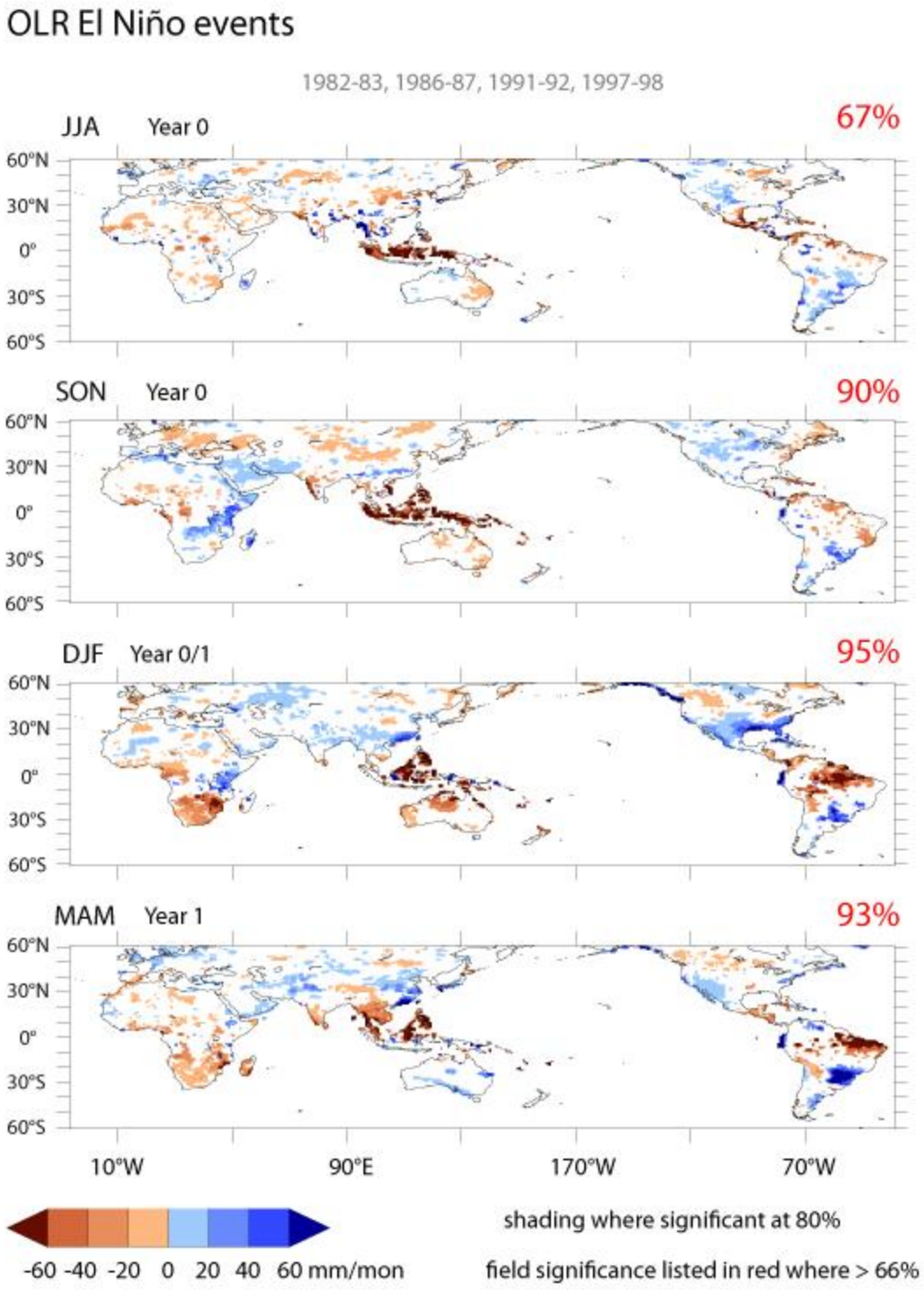

Figure 9: OLR El Niño event composite precipitation anomaly. Shading where amplitudes are significant locally at the 80% confidence level. Field significance listed in red.

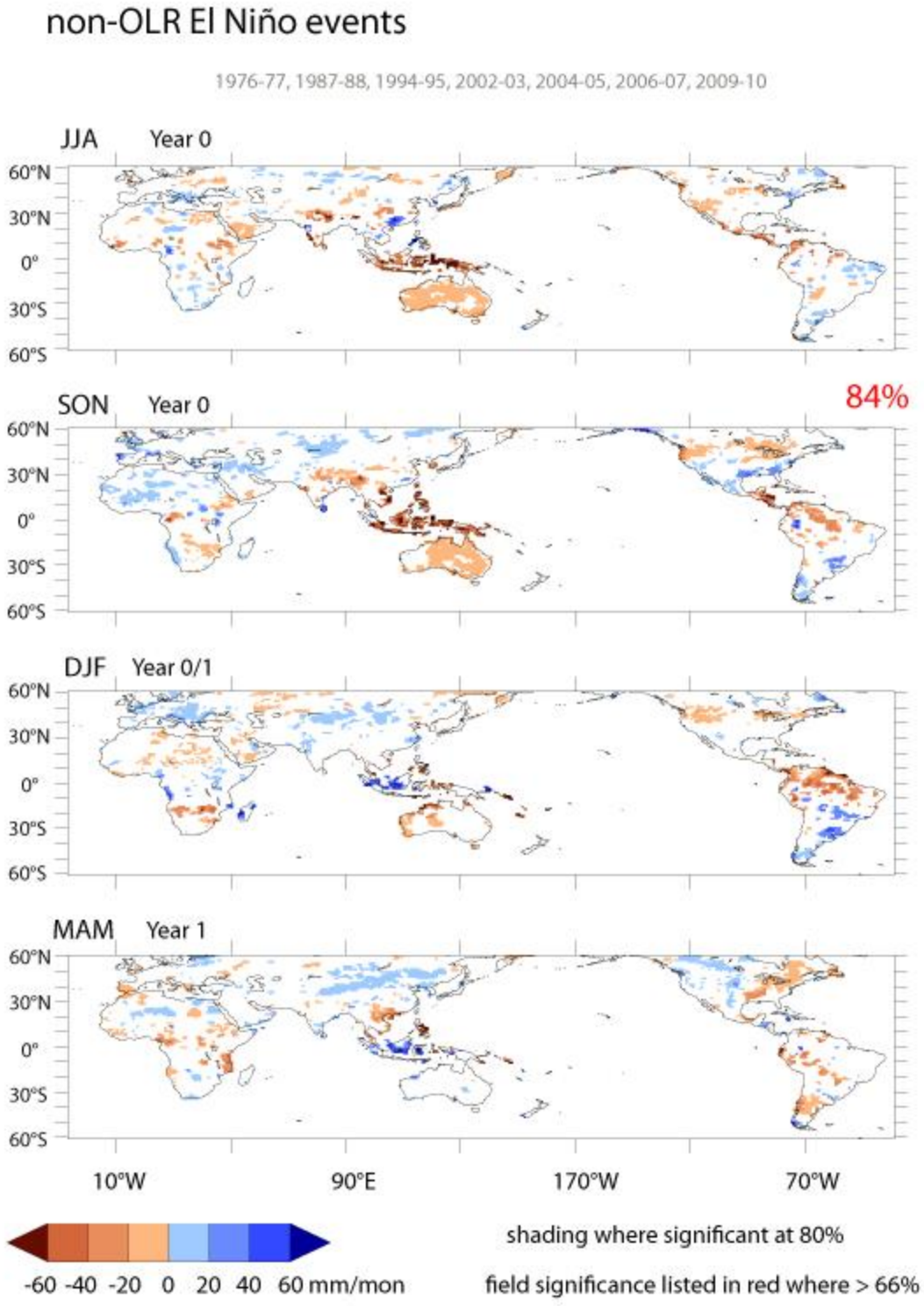

857

858 Figure 10: The non-OLR El Niño event composite precipitation anomaly. Shading where

859 amplitudes are significant locally at the 80% confidence level. Field significance listed in red.

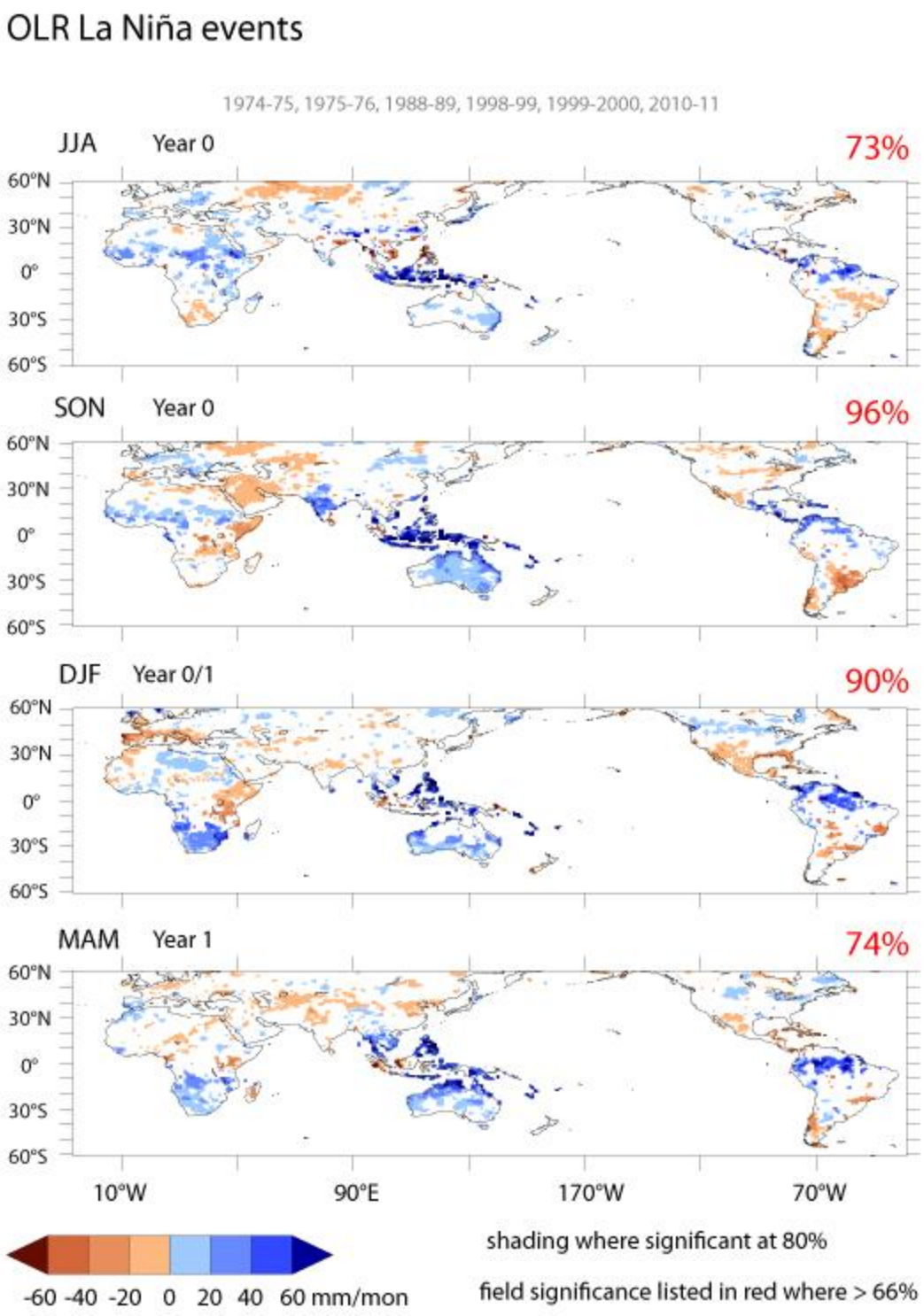

Figure 11: The OLR La Niña event composite precipitation anomaly. Shading where amplitudes are significant locally at the 80% confidence level. Field significance listed in red.

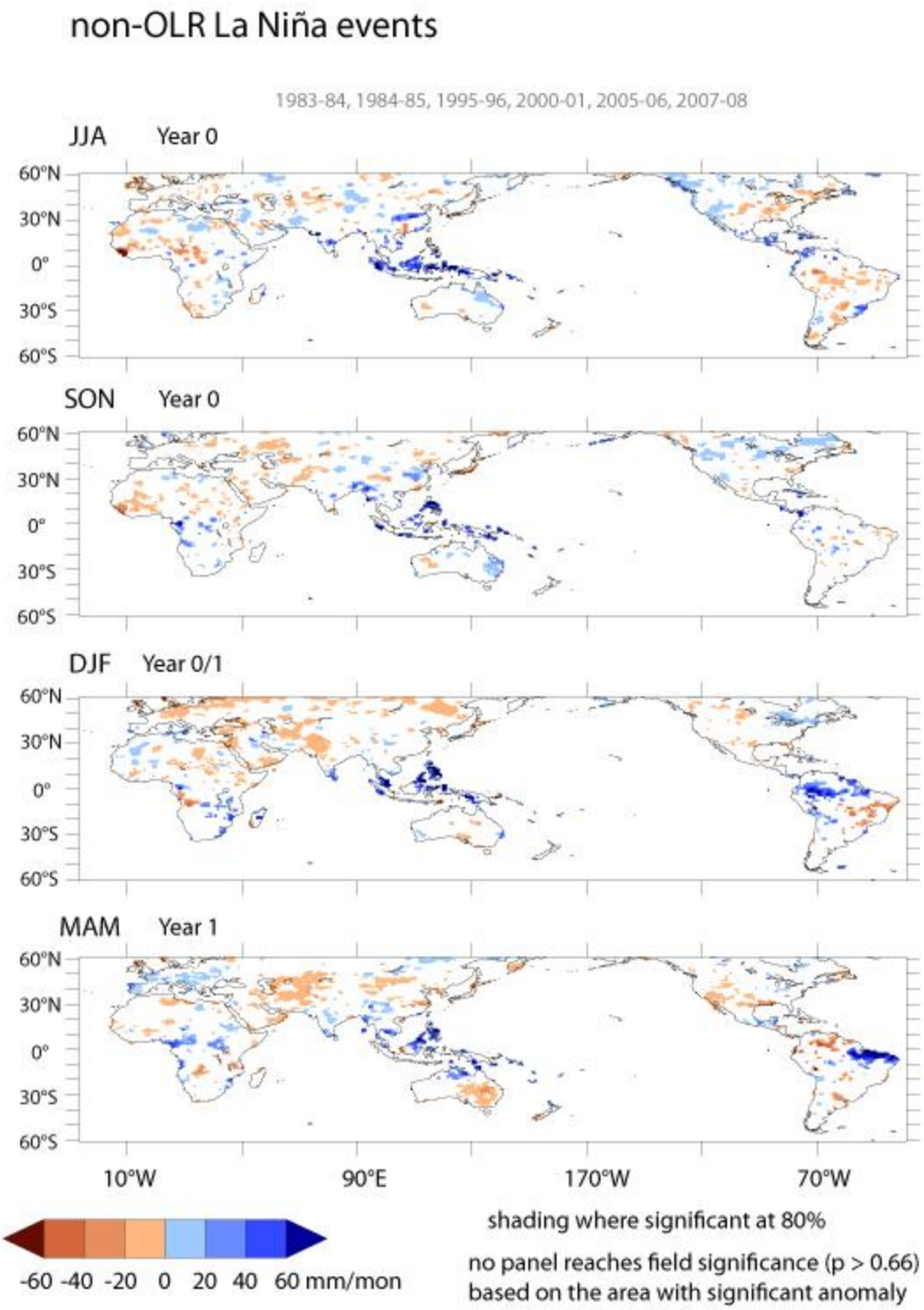

Figure 12: The non-OLR La Niña event composite precipitation anomaly. Shading where amplitudes are significant locally at the 80% confidence level. Field significance listed in red.

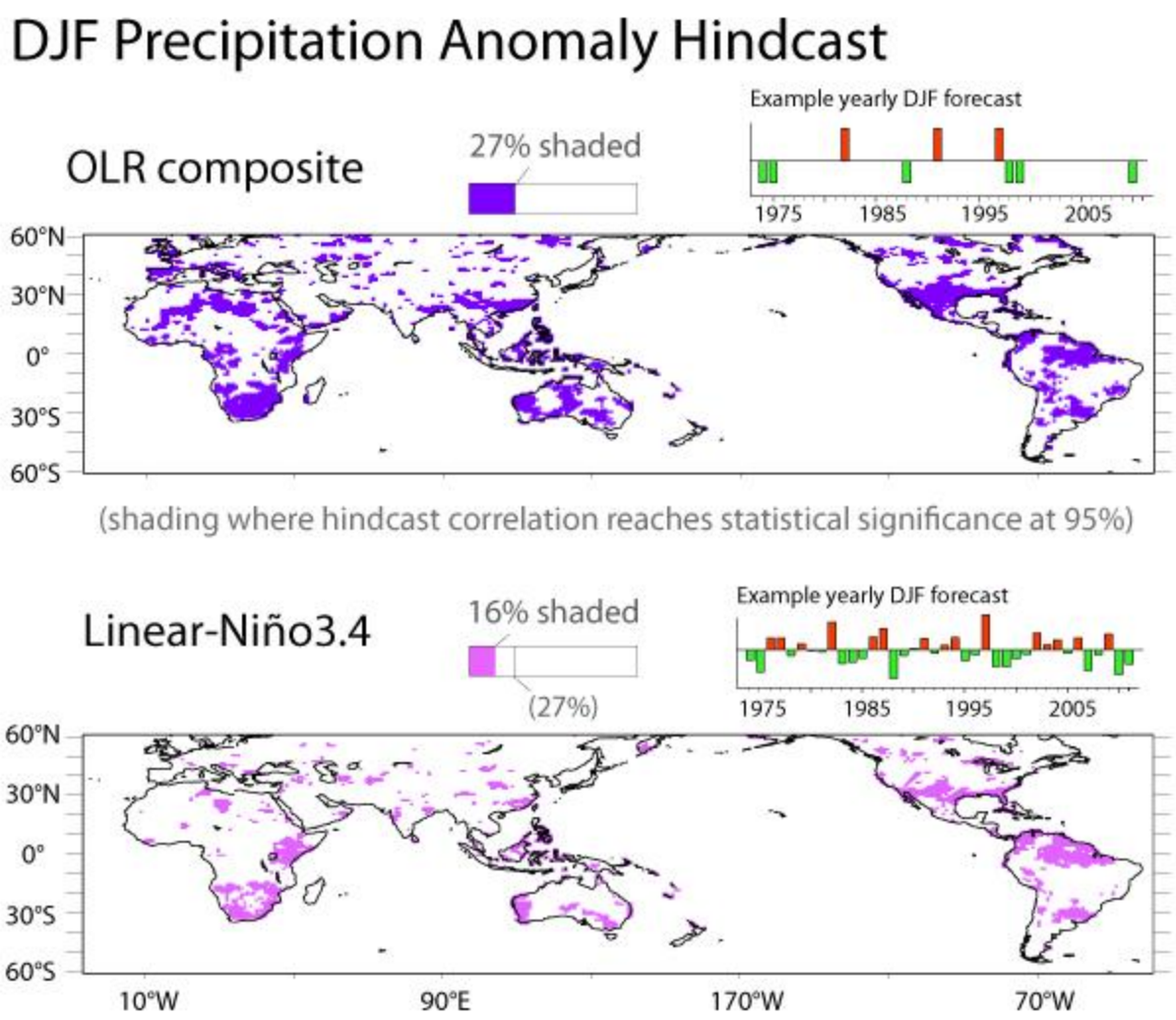

866
867

868 Figure 13. DJF precipitation anomaly hindcast results. Period 1974-2011. Upper panel:
869 Shading where OLR-hindcast anomaly correlation is statistically significant at the 95% level.
870 27% of the land is shaded. In the OLR-hindcast, finite (non-zero) anomalies are only specified
871 in the hindcast in the 9 years identified by the OLR indices prior to boreal winter. The anomaly
872 correlation, however, is computed over all years. Lower panel: Shading where the linear-
873 regression hindcast anomaly correlation is statistically significant at the 95% level. In this case,
874 only 16% of the land is shaded, even though finite anomalies are specified in each year.

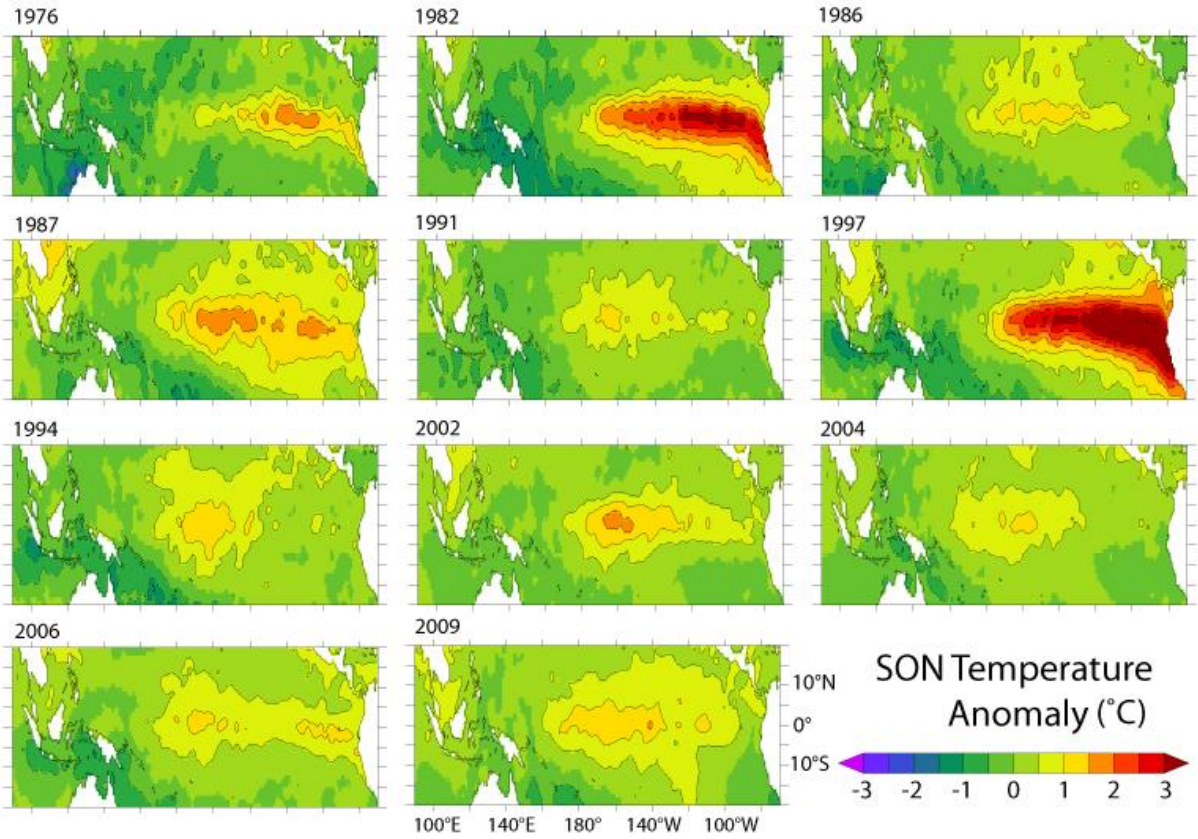

875

876 Figure 14. SON-averaged SSTA in the tropical Pacific in the years with El Niño status based on

877 the NOAA Historical ENSO definition (1974-2011).

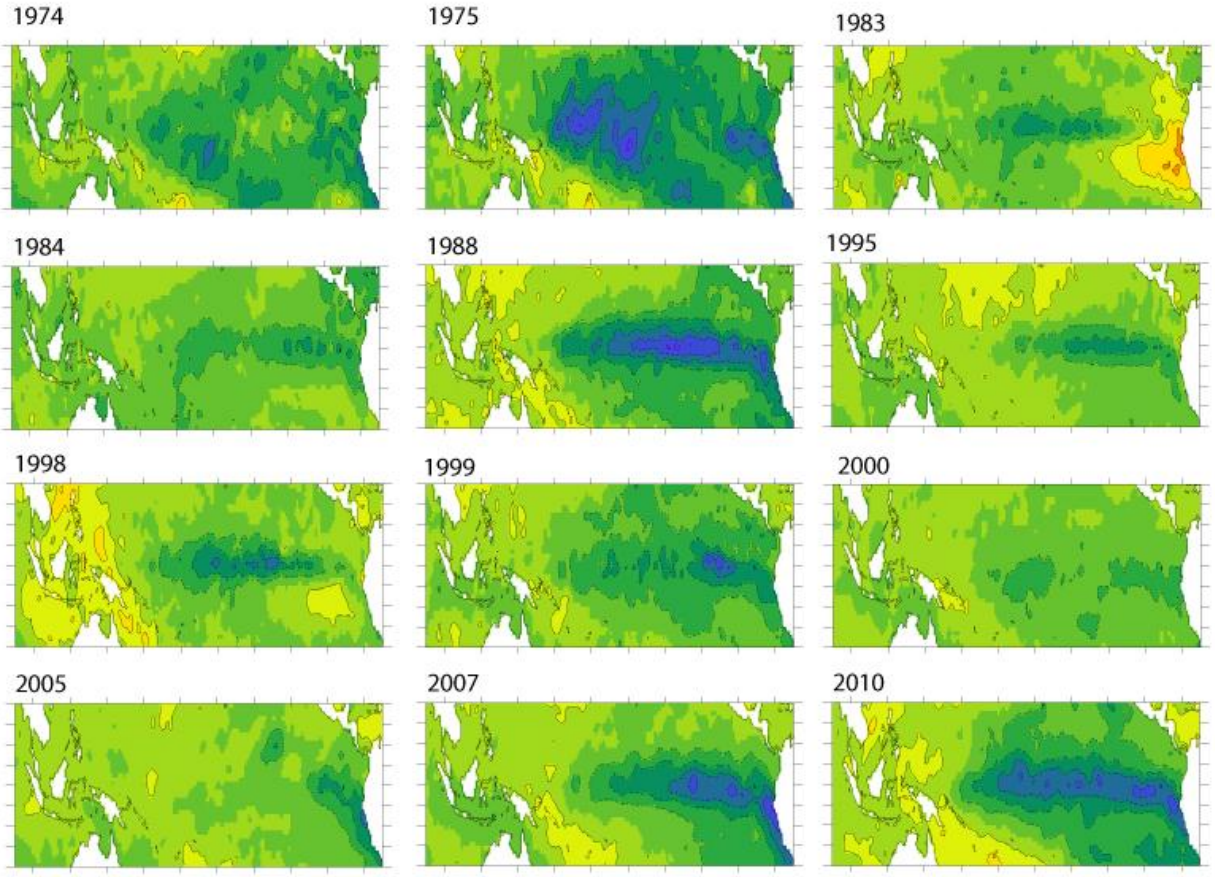

Figure 15. SON-averaged SSTA in the tropical Pacific in the years with La Niña status based on the NOAA Historical ENSO definition (1974-2011).

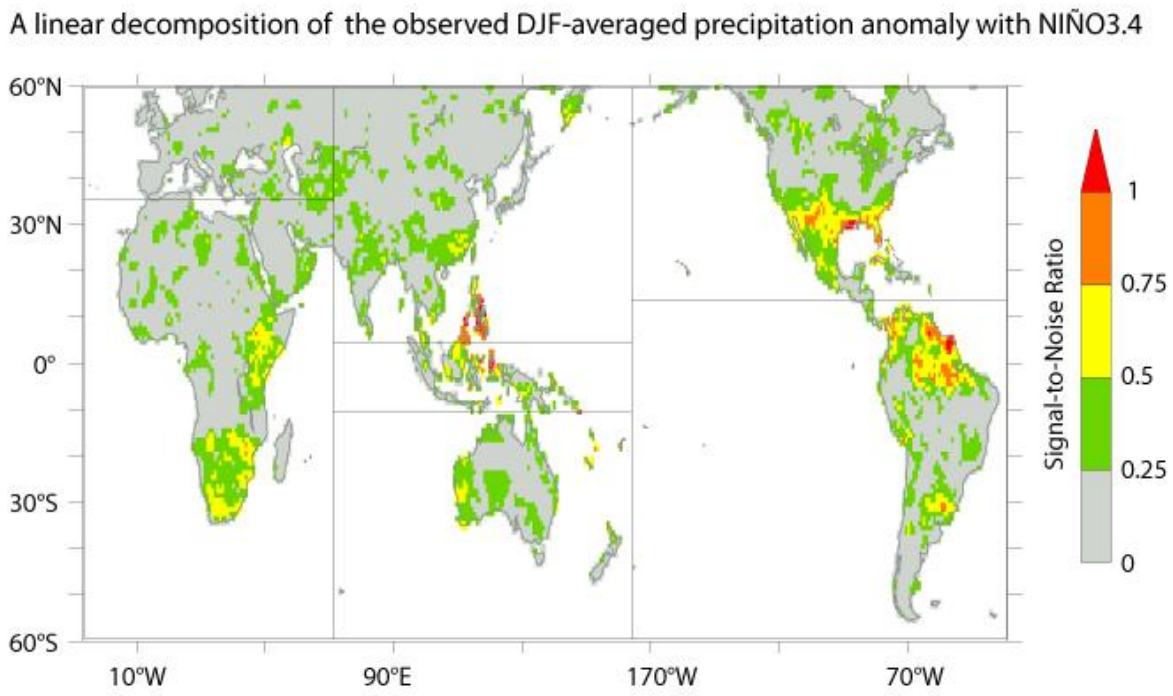

881

882 Figure 16. The "signal-to-noise" ratio for DJF-averaged land precipitation anomaly based on a

883 linear regression with DJF-averaged NIÑO3.4 SSTA.

884